

Microensing Events in Five Years of Photometry from the Zwicky Transient Facility

RUOCHENG ZHAI,^{1,2} ANTONIO C. RODRIGUEZ,³ CASEY Y. LAM,⁴ ERIC C. BELLM,⁵ JOSIAH PURDUM,⁶ FRANK J. MASCI,⁷ AND AVERY WOLD⁷

¹*Department of Astronomy, California Institute of Technology, 1200 E. California Blvd, Pasadena, CA 91125, USA*

²*Department of Astronomy, Tsinghua University, Beijing 100084, China*

³*Department of Astronomy, California Institute of Technology, 1200 E. California Boulevard, Pasadena, CA 91125, USA*

⁴*Observatories of the Carnegie Institution for Science, 813 Santa Barbara Street, Pasadena, CA 91101, USA*

⁵*DIRAC Institute, Department of Astronomy, University of Washington, 3910 15th Avenue NE, Seattle, WA 98195, USA*

⁶*Caltech Optical Observatories, California Institute of Technology, 1200 E. California Blvd, Pasadena, CA 91125, USA*

⁷*IPAC, California Institute of Technology, 1200 E. California Blvd, Pasadena, CA 91125, USA*

ABSTRACT

Microensing has a unique advantage for detecting dark objects in the Milky Way, such as free floating planets, neutron stars, and stellar-mass black holes. Most microensing surveys focus towards the Galactic bulge, where higher stellar density leads to a higher event rate. However, microensing events in the Galactic plane are closer, and take place over longer timescales. This enables a better measurement of the microensing parallax, which serves as an independent constraint on the mass of the dark lens. In this work, we systematically searched for microensing events in Zwicky Transient Facility (ZTF) Data Release 17 from 2018–2023 in the Galactic plane region $|b| < 20^\circ$. We find 124 high-confidence microensing events and 54 possible events. In the event selection, we use the efficient `EventFinder` algorithm to detect microensing signals, which could be used for large datasets such as future ZTF data releases or data from the Rubin Observatory Legacy Survey of Space and Time (LSST). With detection efficiencies of ZTF fields from catalog-level simulations, we calculate the mean Einstein timescale to be $\langle t_E \rangle = 51.7 \pm 3.3$ days, smaller than previous results of the Galactic plane to within $1.5\text{-}\sigma$. We calculate optical depths and event rates, which we interpret with caution due to the use of visual inspection in creating our final sample. With two years of additional ZTF data in DR17, we have more than doubled the amount of microensing events (60) found in the three-year DR5 search and found events with longer Einstein timescales than before.

1. INTRODUCTION

Dark celestial objects, such as stellar remnants and exoplanets, are challenging to probe by typical astronomical methods involving observing their electromagnetic radiation. However, their gravitational fields bend the light passing by them, through a process called gravitational lensing (Einstein 1936; Paczyński 1986). Objects of large scales, like galaxy clusters, can produce strong distortion on the images of background sources, producing arcs or distorted galaxies on the image in an effect called “strong lensing”. Though for stellar mass objects, we can not resolve how they affect the images of the background point sources subject to the resolution limit. Microensing is the regime of gravitational lensing where the individual images are unresolved by the observer,

and can enables constraints to be placed on the properties of dark lenses in our Galaxy by observing light curves of sources (Paczynski 1986, 1996; Mao & Paczynski 1991).

A microensing events is detectable when the source trajectory is at or less than the order of the Einstein radius:

$$\theta_E = \sqrt{\kappa M \pi_{\text{rel}}}, \quad (1)$$

where $\kappa = 8.14 \text{ mas } M_\odot^{-1}$, M is the mass of the lens, and $\pi_{\text{rel}} = 1 \text{ au } (1/D_L - 1/D_S)$ is the relative parallax between the lens and the source. The microlens parallax $\pi_E = \pi_{\text{rel}}/\theta_E$ is introduced to project the motion of the observer to the lens plane. Its direction takes that of the source proper motion, so that the microlens parallax vector is:

$$\boldsymbol{\pi}_E = (\pi_{E,N}, \pi_{E,E}) = \frac{\pi_{\text{rel}} \boldsymbol{\mu}_{\text{rel}}}{\theta_E \mu_{\text{rel}}}. \quad (2)$$

By analyzing the source trajectory observed in the lens plane, π_{rel} can be constrained (Gould 2004). In the situation of observing the same event both on the Earth and a satellite, the

different source trajectory they see can also be scaled by π_E (Gould 1994; Zang et al. 2020). For events only having been observed on the Earth, observing the microlens parallax is most likely for events with longer Einstein timescales. Mróz et al. (2020) showed that the average Einstein timescales ($t_E = \theta_E/\mu_{\text{rel}}$) of Galactic plane events are longer ($t_E \sim 60$ days) than bulge ones ($t_E \sim 20$ days), suggesting that Galactic plane events are more likely to show detectable parallax effects.

However, since microlensing requires the close alignment between the lens and the source, observing a denser field is more profitable, where chances are greater that one star will pass near the line of sight of another. Thus, high cadence searches like Korea Microlensing Telescope Network (KMTNet, Kim et al. 2016) and Microlensing Observations in Astrophysics (MOA; Sumi et al. 2016) mainly focus on the Galactic bulge microlensing events. Optical Gravitational Lensing Experiment (OGLE; Udalski et al. 2015), however, covers a wide range of sky, observing the Galactic bulge, part of the Galactic plane, and the Small/Large Magellanic Clouds. It showed that microlensing event rate towards the Galactic bulge is at the order $10^{-5} \text{ year}^{-1}$ (Mróz et al. 2019), while only $10^{-6} \text{ year}^{-1}$ towards the Galactic plane (Mróz et al. 2020). Rodriguez et al. (2022) conducted a systematic search on the archive of Zwicky Transient Facility (ZTF) Data Release 5 (DR5) focusing on the Northern Galactic plane, finding a total of 60 microlensing events, with mean Einstein timescale $\langle t_E \rangle = 61.0 \pm 8.3$. Medford et al. (2023) independently carried out a search for microlensing events in ZTF DR5 and found 60 events. The mean timescale of Rodriguez et al. (2022) is consistent with the result of Mróz et al. (2020) from events in the Southern Galactic plane.

ZTF DR5 covered approximately 3 years of photometric data, from 2018 to 2021, whereas in this study we use ZTF DR17, which covers approximately 5 years of data through 2023. It enables us to analyze newly transpired microlensing events and further study ones that could have begun brightening during the baseline of DR5, but did not return to quiescence until after the end of DR5.

In Section 2, we describe the ZTF data archive. In section 3, we introduce our methodology to select and analyze microlensing events. In section 4, we perform simulation to calculate detection efficiencies and the mean Einstein timescale. We discuss the microlensing optical depth and event rate from our sample.

2. DATA

ZTF is a time-domain survey using the Samuel Oschin 48 inch telescope with a 47 deg^2 field-of-view camera at Palomar Observatory (Graham et al. 2019; Masci et al. 2019; Bellm et al. 2019a; Dekany et al. 2020). ZTF carries out a public survey on the entire northern sky in g and r bands

(Bellm et al. 2019b; Kupfer et al. 2021) with 3-day cadence in Phase I (first year) (Bellm et al. 2019a) and 2-day cadence in Phase II. We make use of ZTF partnership data which is not currently publicly available, but its inclusion does not strongly impact the final sample of events or alter model parameters. Such data will be published elsewhere in the near future. The pixel size of ZTF camera is $1''$, and the average delivered image quality is $2''.00$ at FWHM.

ZTF Data Release 17 contains public survey data up to 9 March 2023, and private data prior to 6 November 2021, both starting from 17 March 2018. We use all available data in the Galactic plane ($|b| < 20^\circ$), accessing them from Kowalski¹ datastore (Dyev et al. 2019) query tool through the Python package `penquins`² developed for the ZTF collaboration. Light curves have a photometric precision from 0.01 mag at 14 mag up to 0.1-0.2 mag at 20-21 mag for the faintest objects. Because of the Galactic reddening, we start with analyzing 565,054,933 light curves with at least 30 points in 196 fields of r -band data.

3. METHODS

The point-source point-lens (PSPL) model describes the simplest microlensing events involving a single source and a single lens. The magnified flux at a certain moment is:

$$F(t) = \begin{cases} A(t; t_0, u_0, t_E) f_s + f_b & \text{static} \\ A(t; t_0, u_0, t_E, \pi_{E,N}, \pi_{E,E}) f_s + f_b & \text{parallax,} \end{cases} \quad (3)$$

in which t_0 is the time when the source aligns closest to the lens, u_0 is the closest distance normalized to the Einstein radius θ_E , the Einstein timescale t_E is how long it takes the source to cover a distance of the Einstein radius, f_s is the source flux, and f_b is the blended flux due to light from the lens and/or unrelated sources of light within the seeing disk. With a (t_0, u_0, t_E) set, f_s and f_b can be deduced from a linear regression based on the light curve. Thus, we must search for the best parameters in the 3-dimensional space of (t_0, u_0, t_E) . However, considering the great amount of data in ZTF DR17, we need to first search for possible microlensing signals in light curves, which means they resemble a PSPL photometric signature. Then we fit them to obtain reasonable PSPL parameters. For those light curves having gone through the above cuts, we will visually inspect them in multi-band data to confirm whether they are microlensing events. Here we use `MulensModel`³ (Poleski & Yee 2019) to calculate the magnification of and fit the PSPL model.

¹ <https://github.com/dmitrydyev/kowalski>

² <https://github.com/dmitrydyev/penquins>

³ <https://rpoleski.github.io/MulensModel/index.html>

3.1. Skewness-Von Neumann Space

Similar to the former work [Rodriguez et al. \(2022\)](#), we first calculate the skewness γ and Von Neumann statistic η of all r -band light curves in DR17. They are defined as:

$$\begin{aligned}\gamma &= \sum_{i=1}^N \frac{(x_i - \bar{x})^3}{N\hat{\sigma}^3}; \\ \eta &= \sum_{i=2}^N \frac{(x_i - x_{i-1})^2}{(N-1)\hat{\sigma}^2}.\end{aligned}\quad (4)$$

Here x is a sequence of data, i.e., the magnitude in our case, and $\hat{\sigma}$ is the sample standard deviation. Skewness γ goes negative as the brightening signals appear in a light curve (magnitude becomes smaller). Von Neumann statistic η symbolizes the significance of long-term deviations from the baseline.

Based on the microlensing events confirmed by [Rodriguez et al. \(2022\)](#), we calculated the γ and η of their DR17 light curves to develop our cuts in the skewness-Von Neumann space:

$$\gamma < 0; \log_{10}(-\gamma) > 3 \log_{10} \eta + 0.3. \quad (5)$$

3.2. EventFinder Algorithm

[Kim et al. \(2018\)](#) developed the EventFinder algorithm, simplifying the magnified flux to only determined by $(t_0, t_{\text{eff}} \equiv u_0 t_E)$, while u_0 is constrained to high-magnification ($u_0 \rightarrow 0$) or $u_0 = 1$, corresponding to $j = 1, 2$, respectively. Moreover, t_0, t_{eff} only takes discrete values, approximating light curves:

$$\begin{aligned}F(t) &= f_1 A_j [Q(t; t_0, t_{\text{eff}}) + f_0]; \\ Q(t; t_0, t_{\text{eff}}) &\equiv 1 + \left(\frac{t - t_0}{t_{\text{eff}}}\right)^2, \\ (j &= 1, 2); \end{aligned}\quad (6)$$

where:

$$\begin{aligned}A_{j=1} &= Q^{-1/2} \\ A_{j=2} &= \frac{Q + 2}{Q(Q + 4)}.\end{aligned}\quad (7)$$

When $u_0 \rightarrow 0$, $f_1 \rightarrow F_{\text{max}}$ and when $u_0 = 1$, $(f_1, f_0) = (f_s, f_b)$.

We adopt 2-D grids of (t_0, t_{eff}) from [Kim et al. \(2018\)](#), conducting a linear regression to decide the two flux parameters to detect whether a light curve has a signal similar to microlensing events. Also, the EventFinder helps to determine the initial guess of the PSPL model fitting. We define:

$$\Delta\chi^2 = \left(\frac{\chi_{\text{flat}}^2}{\chi_{\text{mulens}}^2} - 1\right) N_{\text{window}}, \quad (8)$$

in which we choose a window of $(t_0 - 5t_{\text{eff}}, t_0 + 5t_{\text{eff}})$, and χ_{flat}^2 and χ_{mulens}^2 are calculated with a flat model and

an EventFinder microlensing model, respectively:

$$\chi_{\text{flat/mulens}}^2 = \sum_{i=1}^N \left(\frac{F_i - F_{\text{model}}}{\sigma_i}\right)^2 \quad (9)$$

We set a $\Delta\chi^2 > 200$ threshold by calculating DR5 confirmed events.

To remove light curves of variable stars, we calculated the reduced chi-squared outside the window:

$$\chi_{\text{out}}^2 = \frac{1}{N_{\text{out}} - 1} \sum_{i=1}^{N_{\text{out}}} \left(\frac{F_i - \bar{F}}{\sigma_i}\right)^2. \quad (10)$$

Here the window is at least 360 days. That is if $10t_{\text{eff}} < 360$ days, we use a 360-day window to calculate χ_{out}^2 . We set a threshold of $\chi_{\text{out}}^2 < 4$ by calculate χ_{out}^2 of events from [Rodriguez et al. \(2022\)](#).

3.3. PSPL Model Fitting

After selecting events by the EventFinder and estimating (t_0, t_{eff}) of a light curve, we set u_0 calculated from the magnification derived from the maximum and minimum flux of it as the initial guess of PSPL model fitting. We use the Nelder-Mead method to find the best-fit parameters.

We implement several cuts based on the PSPL best-fit model. First, we define a lensing window of 360 days centered at t_0 . We remove light curves with fewer than 6 points within the lensing window, as was done in [Mróz et al. \(2017\)](#). Also, light curves with a magnitude amplitude less than 0.2mag are excluded since they are often false positives (e.g. Be star outbursts). To decide whether the PSPL model fits well, we consider reduced chi-squared within the window as well as of the whole light curve:

$$\chi_{\text{red}}^2 = \frac{1}{N - \text{d.o.f}} \sum_{i=1}^N \left(\frac{F_i - \bar{F}}{\sigma_i}\right)^2. \quad (11)$$

With the confirmed events in DR5, we set a $\chi_{\text{red}}^2 < 4$ threshold for both within the lensing window and the whole light curve. Lastly, we choose the light curves, of which $t_0 \pm 0.3t_E$ is fully in data, ensuring events that are rising but don't have a decline covered by DR17, or vice versa, don't make the final sample.

3.4. Multi-band Modeling

After the PSPL model fitting cuts, we visually inspect all events having passed and select events with significant microlensing features. Also, ZTF data exhibit some systematic false positives due to imaging artifacts or calibration errors. These false positives can be distinguished by their appearance in multiple nearby lightcurves. Thus we manually remove them. For the candidates left, we tried to acquire multi-band data for all of them. ZTF typically observes an object

Table 1. Cuts on ZTF DR17 light curves

Criteria	Remarks	Number Left
All light curves in ZTF DR17	Light curves with more than 30 points.	565,054,933
Step 1: skewness-Von Neumann Space		
$\gamma < 0$; $\log_{10}(-\gamma) > 3 \log_{10} \eta + 0.3$	Light curves with significant brightening signals.	805,088
Step 2: EventFinder algorithm		
$\Delta\chi^2 > 200$	The EventFinder microlensing model fits well in the EventFinder window.	
$\chi_{\text{out}}^2 < 4$	Light curves that are flat outside the EventFinder window.	328,086
Model converges	<code>scipy</code> optimization of the PSPL model returns a successful status.	136,939
Step 3: PSPL modeling		
$N_{\text{pts,lens}} \geq 6$	Enough points within the lensing window.	
amplitude $\geq 0.2\text{mag}$	Remove small-rise false positives.	
$\chi_{\text{red,lens}}^2 < 4$	PSPL fits well in the lensing window.	
$\chi_{\text{red,whole}}^2 < 4$	PSPL fits for the whole light curve.	
$t_0 \pm 0.3t_E$ fully in data	Remove events with baseline outside DR17 data.	3,201
Visual inspection	Choose light curves with microlensing signatures.	321
Multi-band data analysis	Fit with multi-band data in DR17.	
High-confidence	Objects that are confirmed as microlensing events.	124
Possible	Objects that have microlensing features, but cannot be confirmed.	54

NOTE—Our automatic selection methodology includes three steps: 1. skewness-Von Neumann Space; 2. EventFinder algorithm; 3. PSPL modeling. Of the 124 high confidence and 54 possible events, 51 are discovered in the ZTF DR5 search (Rodríguez et al. 2022).

in three bands: g , r , and i . However, for most objects, i -band observation only covers a short duration, so we abandon the i -band data of most candidates. Only those data with strong microlensing signals are kept. Because ZTF fields can overlap, we use data from all fields at the position of a given event for multi-band modeling, trying to constrain parameters better.

By introducing multi-band data into the fitting, we can remove those events with strong asymmetry and differences in g -band and r -band. These events are typically dwarf novae or supernovae. Also, we discard events with only half of the microlensing peak observed, for they cannot be distinguished from false positives (e.g. dwarf nova outbursts, Be star outbursts, supernovae), with only data going down after outbursts. We categorized microlensing events into two kinds, high-confidence and possible. On the one hand, high-confidence events can be confirmed as microlensing events, of which ZTF covered thoroughly over the peak, having large signal-to-noise ratio. On the other hand, because possible events may be only sparsely covered over the peak, suffer from large noise, or lack of enough baseline data, we cannot confirm them.

We show the results of every step of cuts and final microlensing events in table 1. Table 2 and 3 show full lists of high-confidence and possible events.

3.5. MCMC Parameter Exploration

In order to estimate the best values of model parameters, we use Markov Chain Monte Carlo (MCMC) to explore the parameter space and the posterior distribution of all parameters. With the PSPL parameters found by the multi-band analysis, we use the package `emcee` (Foreman-Mackey et al. 2013) to conduct a MCMC analysis on all events we have chosen. Since the MCMC exploration may produce a negative blended flux, we impose a prior on f_b (Mróz et al. 2020):

$$\mathcal{L}_{\text{prior}} = \begin{cases} 1 & f_b \geq 0 \\ \exp\left(-\frac{f_b^2}{2\sigma^2}\right) & f_b < 0, \end{cases} \quad (12)$$

where $\sigma = f_{\text{min}}/3$. f_{min} is the flux corresponding to the magnitude $m = 21$. For the static model, we constrain u_0 to positive considering symmetry. Because the parallax model may have degeneracy in positive and negative u_0 (Gould 2004), we set it free in parallax fitting.

To select events whose parallax model fits better than the static PSPL model, we empirically choose a threshold of

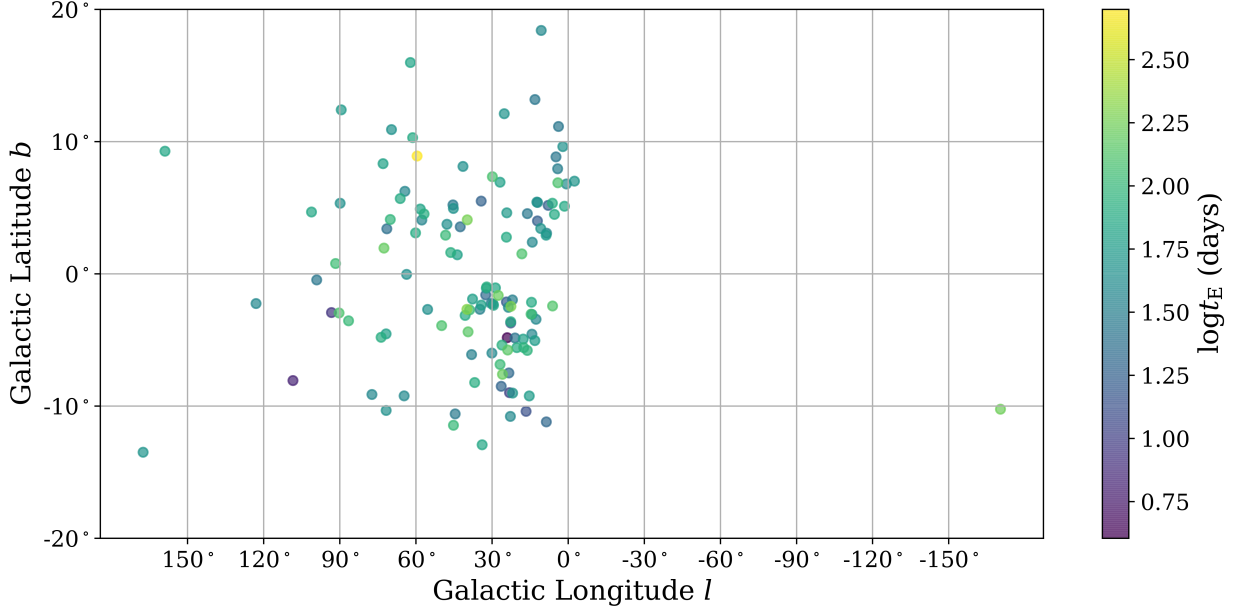


Figure 1. 124 high confidence microlensing events are plotted in Galactic coordinates. Most events are located at low Galactic latitudes and nearby the Galactic bulge. However, some events are located in the anti-bulge direction. Different colors of dots represent the magnitude of the Einstein timescales t_E of the events

$\Delta\chi^2 > 16$. Also, we check the cumulative χ^2 and parameter corner plots of the selected parallax events to ensure it is the lensing window that contributes the lowered χ^2 , as well as check existence of degenerate solutions. For events with degeneracy, we constrain MCMC parameter space based on the corner plot to obtain degenerate solutions separately.

Table 2 shows the MCMC results of all high-confidence events, together with parallax models of some events.

4. RESULTS AND DISCUSSION

4.1. Simulation

To evaluate the ability of ZTF fields to detect microlensing events and the intrinsic distribution of the microlensing event rate, we inject microlensing events onto light curves located in the field where events are detected. For a microlensing event that can be well fitted by the PSPL model, we identify its field. For each field detected with microlensing events, we select 5,000 objects from each quadrant of the 16 CCDs. That is, we generate 320,000 objects per field.

For each object, we select the microlensing parameters from a flat distribution of $(t_0, u_0, \log t_E)$, in range of $t_0 \sim (t_{\min}, t_{\max})$, $u_0 \sim (0, 1)$, $\log t_E \sim (0, 3)$.

As soon as an event is generated, we apply the 3-step algorithm selection methodology in section 3 to it. In this way, we can decide whether a simulated event can be detected by our methodology. We showed detection efficiency curves of fields that are plotted in Rodriguez et al. (2022) Figure 2 as a comparison. We find the maximum value of detection efficiencies of each field is larger, and the detection efficiency curves drops slower on the high Einstein timescale side. The

longer observation time ($\sim 1,786$ days) gives rise to the better detection of the long Einstein timescale events.

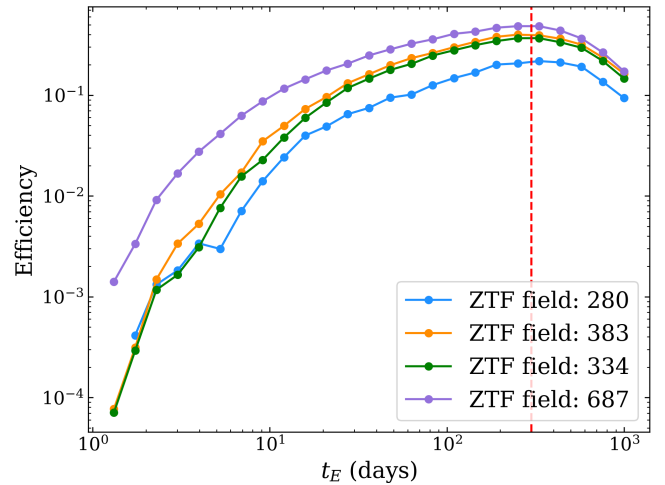


Figure 2. Detection efficiency curves of fields that are shown in Rodriguez et al. (2022), updated by the DR17 objects with longer light curves. The dashed red line marks the t_E where the detection efficiencies drop dramatically in DR5, due to the shorter baseline coverage.

4.2. Einstein Timescale Distribution

To analyze Einstein timescales statistically, we need to first correct the weight of each event we have detected with the detection efficiencies. Each event represents $1/\epsilon(t_{E,i})$ events that actually happen, where $\epsilon(t_{E,i})$ is the detection efficiency of the i th event in its field. We only consider events of non-

negligible detection efficiencies in the following analyses. The mean Einstein timescale is defined as:

$$\langle t_E \rangle = \frac{\sum_i t_{E,i}/\epsilon(t_{E,i})}{\sum_i 1/\epsilon(t_{E,i})}. \quad (13)$$

We find a mean Einstein timescale of $\langle t_E \rangle = 51.7 \pm 3.3$ days, lower than the ZTF DR5 result (Northern Galactic plane) $\langle t_E \rangle = 61.0 \pm 8.3$ days (Rodríguez et al. 2022), as well as OGLE result (Southern Galactic plane) $\langle t_E \rangle = 61.5 \pm 5.0$ days of (Mróz et al. 2020). Nevertheless, our mean Einstein timescale is still much longer than that in the Galactic bulge (~ 20 days, Mróz et al. 2019). We also calculate the log-normal mean Einstein timescale $\langle \log t_E \rangle$ (Wyrzykowski et al. 2015) which is less susceptible to outliers, giving 41.0 ± 2.7 days. The histogram in Figure 3 shows the normalized number of events vs. Einstein timescales.

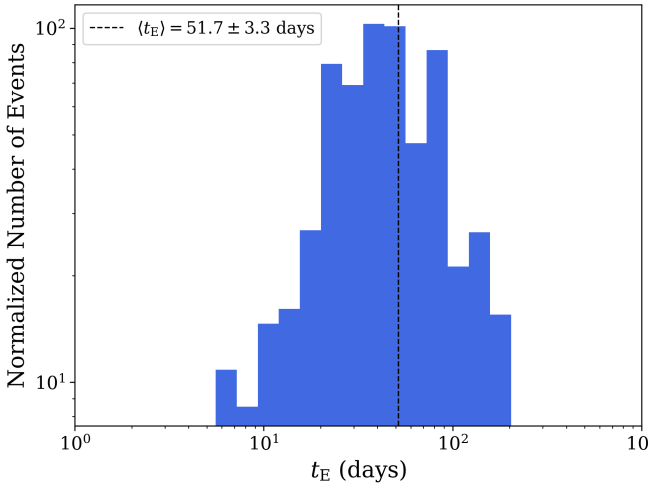


Figure 3. The histogram shows the event number normalized by the reciprocal of detection efficiencies with respect to Einstein timescales (i.e. the corrected histogram of t_E). The vertical dashed line marks the mean Einstein timescale.

To evaluate the dependence of the mean Einstein timescales of different longitudes, we calculate mean Einstein timescales in five bins: $0^\circ < l < 15^\circ$, $15^\circ < l < 25^\circ$, $25^\circ < l < 40^\circ$, $40^\circ < l < 70^\circ$, $70^\circ < l < 180^\circ$, with approximately equal number in each bin. In each bin, we follow the Equation (13), weighting each event by the reciprocal of its detection efficiency. We show the result in the Figure 4. We find low l mean Einstein timescales are shorter than those of medium l , but in the high l bin, the mean Einstein timescale is similar to the shorter t_E found at low l . When checking the high l events, we note there are two events with $t_E < 10$ days in $70^\circ < l < 180^\circ$. If excluding them, the mean Einstein timescale rises significantly, as showed by the orange dashed error bars in Figure 4. This indicates that a small sample of short Einstein

timescale events can have large influence on the mean Einstein timescale since their small detection efficiencies give them large weights when calculating. We plot averaged de-

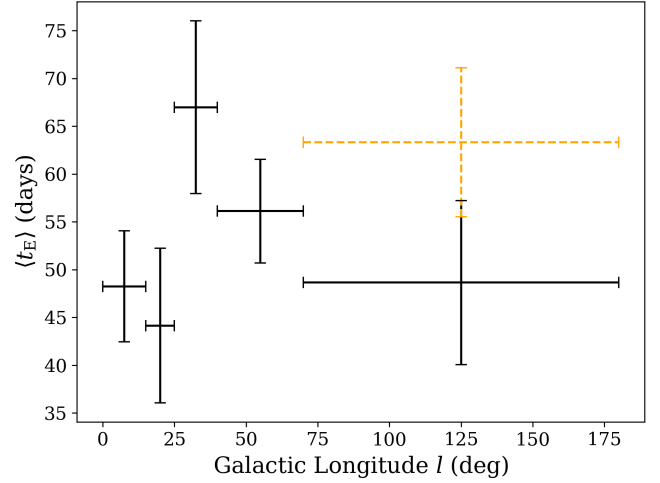


Figure 4. Horizontal error bars represent widths of bins, while vertical error bars are standard deviations of mean Einstein timescales. Orange dashed error bars are calculated without $t_E < 10$ days events.

tection efficiency curves of fields in each bin in Figure 5 to check the performance of ZTF fields of different longitudes. We find that as the longitude increases, the detection efficien-

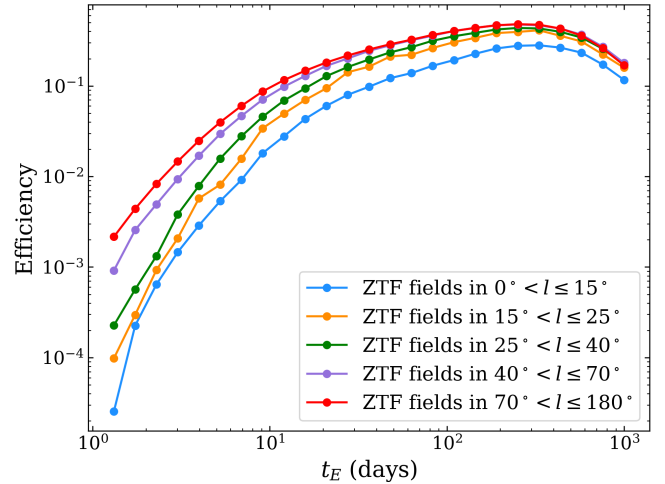


Figure 5. For each Galactic longitude bin, we average over the detection efficiencies of fields. Detection efficiencies rise as the Galactic longitude increases.

cies rises as well at small Einstein timescale side, because of better coverage since the fields are up longer in the sky and fewer sources there. This explained why the two $t_E < 10$ days events with non-negligible detection efficiencies are located at high longitude region. Also, beyond the 3-step algorithm selection methodology itself, we discover that when

visually inspecting microlensing candidates, those with small t_E tend to have little detection on the peak, making it hard to be distinguished from false positives. Hence, with the current cadence of ZTF, we may over estimate mean Einstein timescales.

4.3. Microlensing Optical Depth and Event Rate

The microlensing optical depth is defined as the proportion of sky covered by the Einstein rings of microlensing lenses. Thus, it is proportional to the total Einstein timescales spent by all sources divided by the total survey time (Udalski et al. 1994):

$$\tau = \frac{\pi}{2N_{\text{src}}\Delta T} \sum_i \frac{t_{E,i}}{\epsilon(t_{E,i})}, \quad (14)$$

where N_{src} is the number of sources in the sky region, and ΔT is the duration of the survey: $\Delta T = 1,786$ days.

The microlensing event rate measures the rate of the appearance for a source monitored by ZTF:

$$\Gamma = \frac{1}{N_{\text{src}}\Delta T} \sum_i \frac{1}{\epsilon(t_{E,i})}. \quad (15)$$

The reciprocals of detection efficiencies appear in the two quantities correct the number of microlensing events that our algorithm fails to detect.

Here we calculate the optical depths and event rates at different Galactic coordinates in 7 bins in the Galactic longitude and 6 in the Galactic latitude. Since few events are located in $-180^\circ < l < 0^\circ$ or $|b| > 15^\circ$, we do not calculate optical depths and event rates in these regions. Results are shown in Figure 6, in which the horizontal error bars manifesting the range of bins, while the vertical ones are the errors of measurement defined by Udalski et al. (1994). We fit the optical depths and events rates with exponential decreasing models: $\tau, \Gamma \propto e^{-l/l_0}$, where l_0 is a characteristic length scale. We use the average of Galactic longitudes of fields in each bin to fit. We show the best fit as orange lines in Figure 6. For the optical depth: $\tau_0 = (0.19 \pm 0.04) \times 10^{-6}$, $l_0 = 39.1^\circ \pm 6.5^\circ$; for the event rate: $\Gamma_0 = (0.85 \pm 0.18) \times 10^{-6}$, $l_0 = 39.3^\circ \pm 6.7^\circ$. The characteristic length scale l_0 agrees with that calculated by Mróz et al. (2020) in the Southern Galactic plane (32°), Rodriguez et al. (2022) in the Northern Galactic plane (37°), and the simulations of Sajadian & Poleski (2019) (36°).

Though the changing trends of the optical depth and event rate with respect to the coordinates are consistent with results of OGLE (Mróz et al. 2020), however, the absolute values are discrepant, of which $\tau_0 = 0.77 \pm 0.11$, $\Gamma_0 = 3.02 \pm 0.47$. This discrepancy is most likely raised by the underestimation of source stars in ZTF fields. This is due to stronger blending of sources, caused by the larger plate scale of ZTF compared to OGLE. We conclude that *relative* trends in event rate and

optical depth as a function of Galactic coordinates are consistent between ZTF and OGLE samples, but further work is needed to better count sources in ZTF fields and confidently calculate absolute values.

5. CONCLUSION

We have undertaken a systematic search for microlensing events in the Galactic Plane ($|b| < 20^\circ$) using 5 years of photometric data from ZTF DR17. We found 124 high-confidence events and 54 possible events, doubling the previous amount of microlensing events found in only 3 years of ZTF data (Rodriguez et al. 2022; Medford et al. 2023). For three possible events, we obtained optical spectra with the Hale 200-inch telescope at Palomar Observatory, with details in Appendix A. Their spectra show no evidence of stellar activity or emission lines, which indicate they are associated with true microlensing events. This also demonstrates the potential of spectroscopy to confirm ZTF microlensing events and remove false positives. Interestingly, this suggests that our high confidence sample is very pure, and that events that we have labeled as “possible” may indeed be real.

We performed an injection-recovery test in ZTF fields where we found events, and calculated detection efficiencies. With detection efficiencies as a function of Einstein timescale, we concluded that the mean t_E of our sample is 51.7 ± 3.3 days, shorter than that of previous studies of the Galactic plane.

We then placed our binned our events by Galactic latitude and longitude, finding a characteristic length scale of $\sim 39^\circ$, which is consistent with theoretical predictions and previous surveys. We calculated the microlensing optical depth and event rate as a function of Galactic coordinates, and found that while the trends are similar to that found in OGLE data (Mróz et al. 2020), the overall values are a factor of a few lower. We conclude this is likely due to the difficulty of confidently counting all source stars, due to blending.

We have shown that ZTF can be used to find microlensing events in the Galactic Plane, including those that show a parallax effect which serves as another constraint on the lens mass. Systematic searches of future ZTF data releases, *Gaia* photometry, and the upcoming Rubin Observatory Legacy Survey of Space and Time (LSST) will provide a wealth of microlensing events that will shine new light on the population of dark objects in our Galaxy.

6. ACKNOWLEDGEMENTS

We appreciate the anonymous referee for helping to improve the paper. We thank Shrinivas R. Kulkarni for making this work possible. We thank Shude Mao, Weicheng Zang, and Przemek Mróz for their suggestions on the development of this paper and our methodology. R.Z. acknowledges support by the National Natural Science Foundation of China

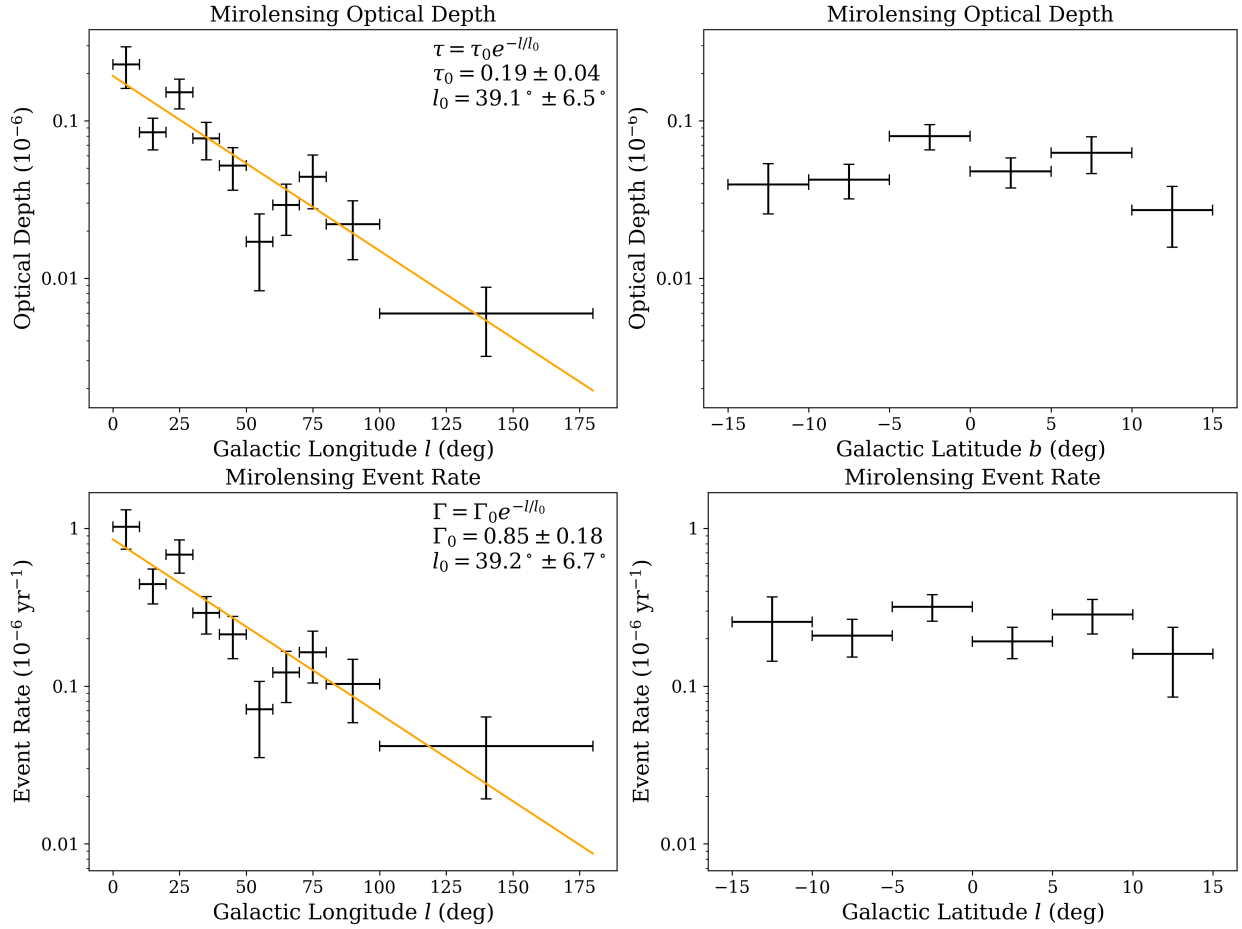


Figure 6. Microlensing optical depth and event rate calculated within bins in the Galactic longitude and latitude. Both optical depth and the event rate drops with the Galactic longitude exponentially, while nearly stable with respect to the Galactic latitude. The minor fluctuation of them on the Galactic latitude is similar to results in Figure 6. of Mróz et al. (2020).

(Grant No. 12133005). A. C. R. acknowledges support from an NSF Graduate Research Fellowship. C. Y. L. acknowledges support from a Carnegie Fellowship and a Harrison Fellowship.

We acknowledge the Tsinghua Astrophysics High-Performance Computing platform at Tsinghua University for providing computational and data storage resources that have contributed to the research results reported within this paper. We are grateful to the staff of Palomar Observatory for their work in helping us carry out our observations.

Based on observations obtained with the Samuel Oschin Telescope 48-inch and the 60-inch Telescope at the Palomar Observatory as part of the Zwicky Transient Facility

project. ZTF is supported by the National Science Foundation under Grants No. AST-1440341 and AST-2034437 and a collaboration including current partners Caltech, IPAC, the Weizmann Institute of Science, the Oskar Klein Center at Stockholm University, the University of Maryland, Deutsches Elektronen-Synchrotron and Humboldt University, the TANGO Consortium of Taiwan, the University of Wisconsin at Milwaukee, Trinity College Dublin, Lawrence Livermore National Laboratories, IN2P3, University of Warwick, Ruhr University Bochum, Northwestern University and former partners the University of Washington, Los Alamos National Laboratories, and Lawrence Berkeley National Laboratories. Operations are conducted by COO, IPAC, and UW.

APPENDIX

A. SPECTROSCOPIC OBSERVATIONS

While modeling the photometric signature of microlensing events is often sufficient to confirm their nature, spectroscopy is ultimately the best tool to rule out any false positives. Young star variability and outbursts, dwarf nova outbursts, and Be star

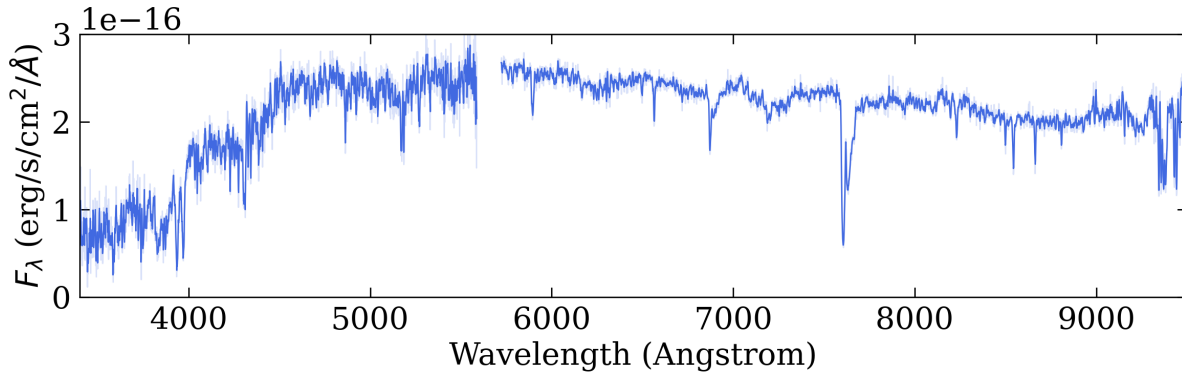


Figure 7. Spectrum of ZTF20acpjzv. No emission lines or indication of stellar activity are present, ensuring us this source is associated with a high confidence microlensing event.

outbursts are just some of the phenomena that may masquerade as microlensing events. For the most part, all of these systems, and other possible false positives would show emission lines in an optical spectrum, whereas the source star in a true microlensing event would simply be a main sequence star. Optical spectroscopy is also useful since the source properties (e.g. stellar type, luminosity, distance) can be constrained. Precise knowledge of these parameters would allow for another constraint that would ultimately lead to a precise measurement of the lens mass.

We obtained optical spectroscopy using the Double Spectrograph (DBSP; Oke & Gunn 1982) on the Hale Telescope on 14 October 2023. We used the 600/4000 grism on the blue side and the 316/7500 grating on the red side. A $1.0''$ slit was used, and the seeing throughout the observation varied between $1.0 - 1.3''$, leading to some slit losses. All P200/DBSP data were reduced with DBSP-DRP⁴, a Python-based pipeline optimized for DBSP built on the more general PyPEIT pipeline (Prochaska et al. 2020). All data were flat fielded sky-subtracted using standard techniques. Internal arc lamps were used for the wavelength calibration and a standard star for overall flux calibration.

We acquired spectra of three of our microlensing candidates to check for emission lines. We purposefully chose events whose light curves showed smaller brightening amplitudes than average in our sample, but nevertheless had a good fit to the PSPL model. Spectra of all three systems reveal them to be ordinary K and M dwarfs, with no significant ($> 3\sigma$) emission lines above the continuum.

B. LISTS OF ALL EVENTS

Here we list all 124 high-confidence events and 54 possible events in Table 2 and Table 3. In the list of the high-confidence events, we also include parallax model results for events who have. We present the ZTF IDs, coordinates, MCMC model parameters, and $\chi^2/\text{d.o.f}$ in the tables. In the tables we show $\text{HJD}' = \text{HJD} - 2450000$ days, while we use HJD when fitting light curves. We provide machine-readable versions of the two tables, with static and parallax models separated.

We show light curves of 4 events as examples in Figure 8. We show one event with a characteristic time scale similar to the mean t_E of our sample, and one event with a particularly long timescale. These events have good coverage throughout the baseline as well as the peak. At the same time, we include 2 events identified as false positives that we manually remove from our samples in Figure 9

⁴ <https://dbsp-drp.readthedocs.io/en/stable/index.html>

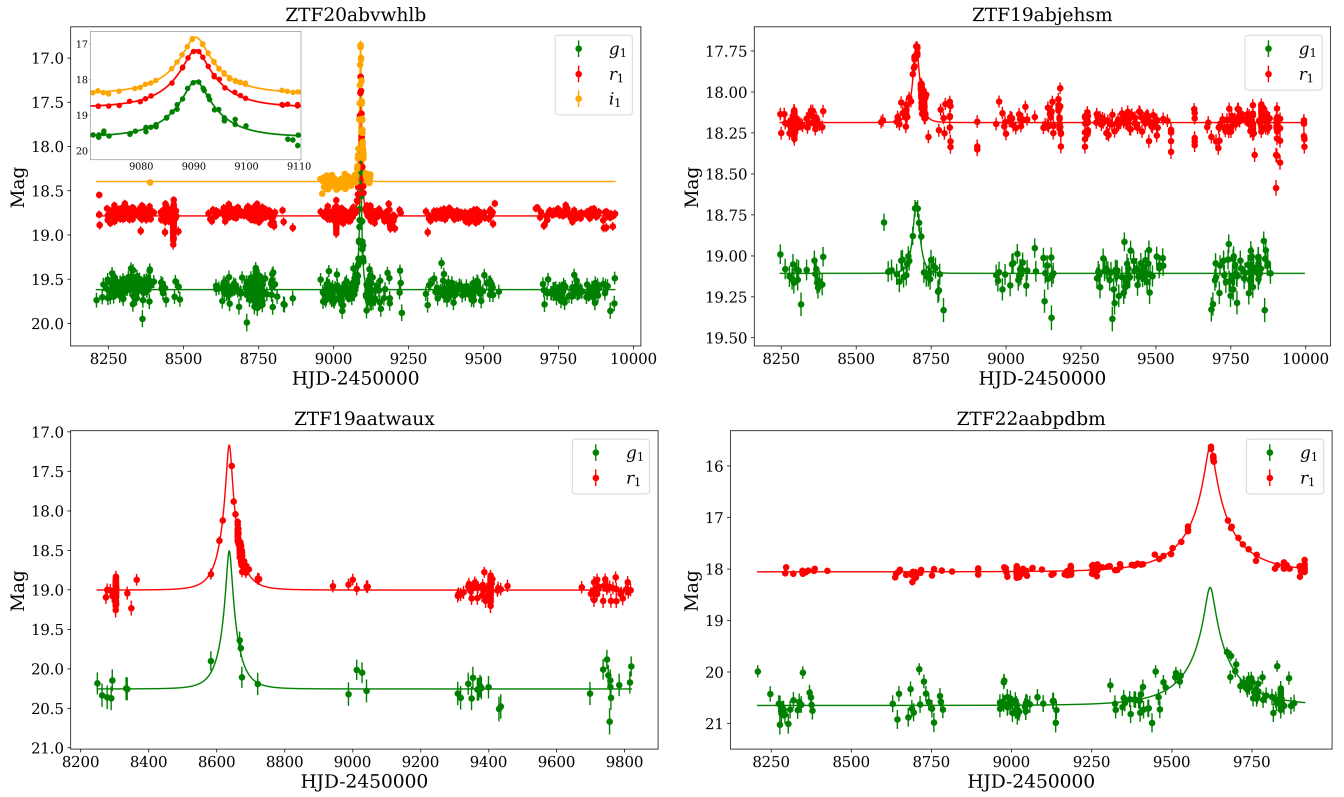


Figure 8. Light curves of ZTF20abvwhlb, ZTF19abjehsm, ZTF19aatwaux, and ZTF22aabpdbm. Einstein timescale of ZTF20abvwhlb is $8.776^{+0.379}_{-0.293}$ days. Einstein timescale of ZTF19abjehsm is $20.625^{+4.910}_{-3.237}$ days. Einstein timescale of ZTF19aatwaux is $51.623^{+7.659}_{-5.228}$ days. Einstein timescale of ZTF22aabpdbm is $162.668^{+14.650}_{-13.015}$ days.

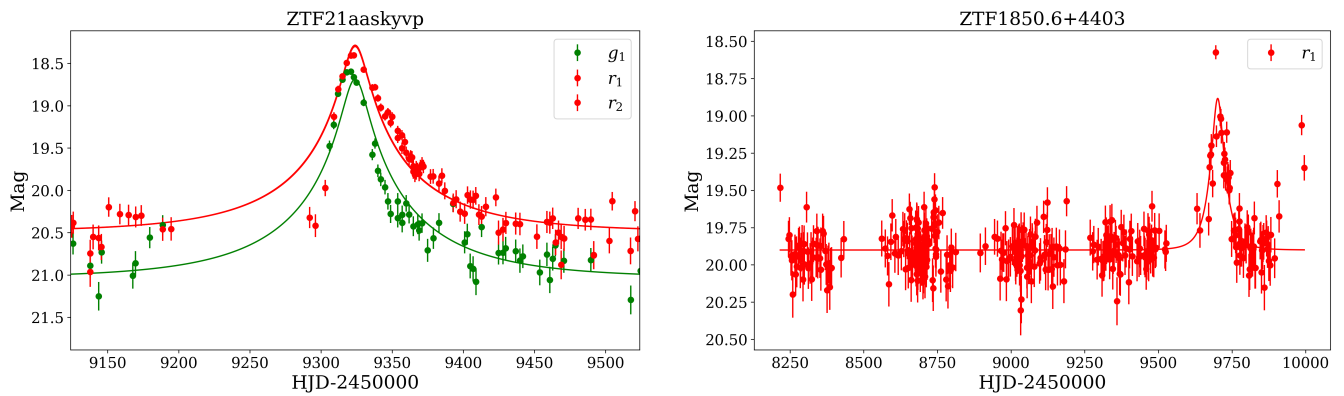


Figure 9. Light curves of two false positives: ZTF21aaskyvp and ZTF1850.6+4403. ZTF21aaskyvp was classified as a supernova (SN 2021icu, Forster et al. 2021). We remove it thanks to the exponential decay and color change in the light curve. ZTF1850.6+4403 has a few outliers at the end of its light curve and has similar shape to many events located far away from each other. Hence, we identify them as false positives.

Table 2. List of High-confidence Microlensing Events in ZTF DR17 with MCMC Parameters

ID	R.A. (J2000)	Decl. (J2000)	t_0 (HJD ¹)	u_0	t_E	$\pi_{E,N}$	$\pi_{E,E}$	r_s (mag)	g_s (mag)	$\chi^2/\text{d.o.f}$
ZTF20abwxmep	12.904570	60.617889	9092.74 ^{+0.88} _{-0.90}	0.48 ^{+0.06} _{-0.10}	41.7 ^{+5.9} _{-3.1}	20.1 ^{+0.3} _{-0.2}	21.6 ^{+0.3} _{-0.2}	1229.7/933
ZTF19adbsiat	65.329219	30.695008	8915.88 ^{+0.72} _{-0.74}	0.68 ^{+0.04} _{-0.06}	50.4 ^{+3.1} _{-1.9}	18.3 ^{+0.2} _{-0.1}	19.3 ^{+0.2} _{-0.1}	1733.5/988
ZTF0527.8+5142	81.950964	51.705438	9445.32 ^{+0.09} _{-0.09}	0.05 ^{+0.00} _{-0.00}	69.6 ^{+2.8} _{-2.7}	19.3 ^{+0.1} _{-0.1}	20.3 ^{+0.1} _{-0.1}	1536.1/877
↑	↑	↑	9443.33 ^{+0.17} _{-0.11}	-0.00 ^{+0.00} _{-0.00}	421.0 ^{+89.5} _{-71.1}	-0.520 ^{+0.073} _{-0.075}	0.060 ^{+0.016} _{-0.013}	19.3 ^{+0.1} _{-0.1}	20.3 ^{+0.1} _{-0.1}	1416.6/875
ZTF20abztmco	82.452721	15.428445	9238.35 ^{+0.26} _{-0.26}	0.23 ^{+0.02} _{-0.02}	172.8 ^{+8.6} _{-8.3}	19.3 ^{+0.1} _{-0.1}	20.6 ^{+0.1} _{-0.1}	2582.4/1180
↑	↑	↑	9236.94 ^{+0.34} _{-0.34}	0.39 ^{+0.01} _{-0.02}	118.3 ^{+3.2} _{-2.1}	0.093 ^{+0.018} _{-0.021}	-0.107 ^{+0.014} _{-0.013}	19.3 ^{+0.1} _{-0.1}	20.6 ^{+0.1} _{-0.1}	2523.1/1178
↑	↑	↑	9236.12 ^{+0.39} _{-0.35}	0.13 ^{+0.03} _{-0.02}	263.7 ^{+47.8} _{-41.6}	-0.003 ^{+0.005} _{-0.005}	-0.003 ^{+0.005} _{-0.005}	19.3 ^{+0.1} _{-0.1}	20.6 ^{+0.1} _{-0.1}	2530.6/1178
ZTF21aadrxr	255.942718	-10.214135	9237.50 ^{+0.09} _{-0.08}	0.06 ^{+0.00} _{-0.00}	39.2 ^{+0.9} _{-0.9}	15.7 ^{+0.0} _{-0.0}	16.9 ^{+0.0} _{-0.0}	1399.3/1257
ZTF19aatwax	258.208394	-27.182025	8637.02 ^{+0.56} _{-0.53}	0.15 ^{+0.04} _{-0.04}	51.6 ^{+7.7} _{-5.2}	19.3 ^{+0.3} _{-0.2}	20.6 ^{+0.3} _{-0.2}	533.1/559
ZTF21aaqsyeh	258.385319	-19.727009	9310.94 ^{+0.35} _{-0.35}	0.40 ^{+0.02} _{-0.04}	27.6 ^{+2.0} _{-1.2}	18.5 ^{+0.2} _{-0.1}	19.4 ^{+0.2} _{-0.1}	2076.8/711
ZTF21abdthbw	258.715905	-21.966701	9382.33 ^{+0.06} _{-0.06}	0.04 ^{+0.01} _{-0.00}	45.9 ^{+4.7} _{-3.9}	20.2 ^{+0.1} _{-0.1}	21.2 ^{+0.1} _{-0.1}	857.9/732
ZTF1721.6-2443	260.395064	-24.721539	9770.27 ^{+0.03} _{-0.02}	0.00 ^{+0.00} _{-0.00}	41.5 ^{+3.4} _{-3.0}	19.0 ^{+0.1} _{-0.1}	20.1 ^{+0.1} _{-0.1}	746.8/673
ZTF19abpxung	260.994091	-20.194962	8713.86 ^{+0.05} _{-0.05}	0.05 ^{+0.01} _{-0.01}	27.7 ^{+1.8} _{-1.5}	19.4 ^{+0.1} _{-0.1}	20.6 ^{+0.1} _{-0.1}	1052.2/880
ZTF22aaknmsp	261.417335	-21.232529	9736.85 ^{+0.21} _{-0.21}	0.11 ^{+0.01} _{-0.02}	33.1 ^{+4.3} _{-2.7}	19.7 ^{+0.2} _{-0.1}	21.5 ^{+0.2} _{-0.1}	433.4/411
ZTF22aakolyk	261.725881	-11.004709	9737.67 ^{+0.13} _{-0.12}	0.22 ^{+0.04} _{-0.03}	26.7 ^{+2.4} _{-2.2}	19.0 ^{+0.2} _{-0.2}	19.8 ^{+0.2} _{-0.2}	1106.9/722
ZTF21aawqeqn	262.325899	-21.875246	9343.11 ^{+0.53} _{-0.57}	0.14 ^{+0.03} _{-0.02}	125.2 ^{+15.2} _{-13.0}	17.8 ^{+0.2} _{-0.2}	19.6 ^{+0.2} _{-0.2}	611.6/355
ZTF21abdikzn	262.411213	-25.010295	9407.11 ^{+0.84} _{-0.85}	0.31 ^{+0.08} _{-0.09}	83.6 ^{+23.1} _{-12.9}	19.6 ^{+0.4} _{-0.3}	21.4 ^{+0.4} _{-0.3}	362.8/298
ZTF19aazhmab	264.957266	-20.894358	8642.29 ^{+0.11} _{-0.14}	0.03 ^{+0.02} _{-0.02}	82.7 ^{+14.8} _{-11.8}	19.7 ^{+0.3} _{-0.3}	20.7 ^{+0.2} _{-0.2}	94.3/85
ZTF21abehtld	265.277131	-22.024187	9375.80 ^{+0.45} _{-0.47}	0.24 ^{+0.02} _{-0.03}	79.4 ^{+7.2} _{-4.1}	18.6 ^{+0.2} _{-0.1}	20.3 ^{+0.2} _{-0.1}	344.3/280
ZTF22aazwyeu	266.027068	-19.565755	9801.27 ^{+0.58} _{-0.53}	0.49 ^{+0.15} _{-0.16}	21.6 ^{+5.7} _{-3.2}	18.1 ^{+0.6} _{-0.4}	19.7 ^{+0.6} _{-0.4}	1108.7/1250
ZTF1752.3-1551	268.066416	-15.860507	9682.24 ^{+0.16} _{-0.13}	0.04 ^{+0.03} _{-0.03}	40.4 ^{+13.8} _{-10.0}	19.7 ^{+0.4} _{-0.4}	20.7 ^{+0.4} _{-0.4}	1088.6/503
ZTF21aavhwjy	268.178174	-15.623007	9352.87 ^{+0.11} _{-0.12}	0.14 ^{+0.01} _{-0.01}	47.4 ^{+2.0} _{-1.8}	17.6 ^{+0.1} _{-0.1}	18.7 ^{+0.1} _{-0.1}	410.3/520
ZTF1753.1-2006	268.285211	-20.114489	8266.61 ^{+0.56} _{-0.59}	0.16 ^{+0.05} _{-0.05}	40.0 ^{+9.2} _{-5.6}	18.5 ^{+0.4} _{-0.3}	21.0 ^{+0.4} _{-0.3}	269.9/345
ZTF20aaukggm	268.528270	-20.022328	8962.00 ^{+1.13} _{-1.61}	0.11 ^{+0.02} _{-0.02}	53.5 ^{+6.3} _{-5.6}	18.2 ^{+0.3} _{-0.3}	20.6 ^{+0.2} _{-0.3}	614.9/401
ZTF20abqkcsf	268.552367	-1.281956	9078.65 ^{+1.80} _{-1.92}	0.14 ^{+0.05} _{-0.05}	55.5 ^{+21.5} _{-9.6}	20.9 ^{+0.6} _{-0.4}	21.9 ^{+0.6} _{-0.4}	642.2/440
ZTF21abehtjv	269.186521	-17.938606	9399.29 ^{+0.19} _{-0.18}	0.22 ^{+0.02} _{-0.02}	48.8 ^{+3.7} _{-3.0}	18.4 ^{+0.1} _{-0.1}	20.1 ^{+0.1} _{-0.1}	622.2/504
ZTF20abkynur	269.342506	-16.534367	9048.38 ^{+0.13} _{-0.12}	0.14 ^{+0.01} _{-0.01}	17.2 ^{+1.1} _{-1.1}	19.7 ^{+0.1} _{-0.1}	21.5 ^{+0.1} _{-0.1}	463.2/236
ZTF22abeflfn	270.864163	-12.808809	9821.76 ^{+0.17} _{-0.16}	0.08 ^{+0.02} _{-0.02}	28.8 ^{+4.2} _{-2.9}	20.2 ^{+0.2} _{-0.2}	22.6 ^{+0.2} _{-0.2}	768.4/370
ZTF19abbwpls	271.842407	-15.547390	8678.40 ^{+0.35} _{-0.35}	0.46 ^{+0.16} _{-0.11}	37.1 ^{+6.7} _{-6.0}	18.2 ^{+0.4} _{-0.5}	20.3 ^{+0.4} _{-0.5}	664.5/579

Table 2 continued

Table 2 (continued)

ID	R.A. (J2000)	Decl. (J2000)	t_0 (HJD')	u_0	t_E	$\pi_{E,N}$	$\pi_{E,E}$	τ_s (mag)	g_s (mag)	$\chi^2/d.o.f$
ZTF19abagvae	272.202031	-24.882547	8719.39 ^{+0.17} _{-0.18}	0.03 ^{+0.00} _{-0.00}	132.5 ^{+8.1} _{-7.6}	17.2 ^{+0.1} _{-0.1}	20.2 ^{+0.1} _{-0.1}	737.5/493
ZTF19aaonska	273.900548	-2.256947	8613.33 ^{+0.29} _{-0.30}	0.32 ^{+0.01} _{-0.01}	62.6 ^{+1.8} _{-1.3}	18.9 ^{+0.1} _{-0.0}	22.0 ^{+0.1} _{-0.1}	1097.6/728
ZTF21abihdde	274.662119	-12.373164	9422.12 ^{+0.57} _{-0.59}	0.10 ^{+0.04} _{-0.03}	132.7 ^{+42.7} _{-27.5}	20.7 ^{+0.4} _{-0.4}	...	1158.2/340
ZTF21abrgqfr	274.713579	-5.681588	9469.89 ^{+0.17} _{-0.17}	0.13 ^{+0.02} _{-0.01}	54.9 ^{+4.1} _{-3.9}	18.9 ^{+0.1} _{-0.1}	21.5 ^{+0.1} _{-0.1}	1818.7/953
ZTF19aaprbng	274.913467	0.591055	8630.96 ^{+1.50} _{-1.54}	0.53 ^{+0.15} _{-0.12}	120.5 ^{+23.1} _{-19.0}	19.3 ^{+0.4} _{-0.4}	20.6 ^{+0.4} _{-0.4}	1765.8/982
ZTF22aalfixa	276.158833	-17.442469	9769.13 ^{+0.52} _{-0.52}	0.31 ^{+0.03} _{-0.04}	80.0 ^{+8.0} _{-4.5}	18.8 ^{+0.2} _{-0.1}	21.7 ^{+0.2} _{-0.1}	502.3/666
ZTF20aaudodap	276.422205	-6.410747	8976.98 ^{+0.16} _{-0.16}	0.14 ^{+0.02} _{-0.02}	76.6 ^{+7.6} _{-6.2}	19.9 ^{+0.1} _{-0.1}	...	862.3/512
ZTF20aawanug	276.484352	-19.624858	8980.87 ^{+0.12} _{-0.12}	0.19 ^{+0.01} _{-0.02}	38.6 ^{+2.1} _{-1.7}	17.5 ^{+0.1} _{-0.1}	19.0 ^{+0.1} _{-0.1}	844.0/931
ZTF20abgrrpjjg	276.919158	-18.041253	9045.10 ^{+0.13} _{-0.13}	0.12 ^{+0.01} _{-0.01}	53.5 ^{+2.7} _{-2.1}	17.6 ^{+0.1} _{-0.1}	19.5 ^{+0.1} _{-0.1}	626.6/351
ZTF21abmnmkl	277.074754	-17.717224	9458.73 ^{+0.56} _{-0.54}	0.29 ^{+0.06} _{-0.05}	110.8 ^{+14.3} _{-12.5}	18.3 ^{+0.2} _{-0.2}	20.4 ^{+0.2} _{-0.2}	703.8/959
↑	↑	↑	9464.37 ^{+7.59} _{-2.60}	0.42 ^{+0.12} _{-0.09}	124.2 ^{+68.5} _{-35.7}	0.537 ^{+0.244} _{-0.356}	0.085 ^{+0.090} _{-0.124}	18.3 ^{+0.2} _{-0.2}	20.4 ^{+0.2} _{-0.2}	686.8/957
ZTF22aawaiui	278.234674	-19.949175	9804.58 ^{+1.06} _{-1.03}	0.51 ^{+0.28} _{-0.20}	54.9 ^{+21.4} _{-13.4}	18.4 ^{+0.8} _{-0.8}	18.8 ^{+0.8} _{-0.8}	465.1/683
ZTF22aalwfkx	278.329469	-18.709197	9777.65 ^{+0.27} _{-0.28}	0.42 ^{+0.05} _{-0.06}	38.5 ^{+3.8} _{-2.5}	16.2 ^{+0.2} _{-0.2}	17.6 ^{+0.2} _{-0.2}	491.6/901
ZTF19acigmif	278.554509	3.654421	8794.83 ^{+0.47} _{-0.48}	0.59 ^{+0.08} _{-0.11}	20.3 ^{+2.9} _{-1.7}	17.8 ^{+0.4} _{-0.2}	19.6 ^{+0.4} _{-0.2}	1341.9/1072
ZTF19aakeacq	279.404621	11.200599	8544.78 ^{+0.59} _{-0.59}	0.57 ^{+0.13} _{-0.13}	47.2 ^{+5.2} _{-3.6}	17.4 ^{+0.3} _{-0.3}	18.2 ^{+0.3} _{-0.3}	1514.0/1275
ZTF19abibzvr	279.567874	-10.709303	8300.96 ^{+0.40} _{-0.38}	0.24 ^{+0.08} _{-0.08}	36.2 ^{+12.4} _{-6.4}	20.7 ^{+0.5} _{-0.4}	...	526.7/527
ZTF22aamzssp	280.288549	-10.396408	9888.30 ^{+0.52} _{-0.52}	0.26 ^{+0.02} _{-0.02}	192.2 ^{+9.9} _{-9.7}	18.0 ^{+0.1} _{-0.1}	20.6 ^{+0.1} _{-0.1}	1262.2/1186
↑	↑	↑	9893.29 ^{+1.13} _{-1.08}	0.36 ^{+0.01} _{-0.01}	162.9 ^{+6.0} _{-5.5}	0.163 ^{+0.021} _{-0.028}	0.140 ^{+0.023} _{-0.025}	18.0 ^{+0.1} _{-0.1}	20.6 ^{+0.1} _{-0.1}	1156.8/1184
ZTF22aawajjj	280.300903	-15.824925	9793.66 ^{+0.28} _{-0.28}	0.16 ^{+0.02} _{-0.02}	61.0 ^{+5.4} _{-4.9}	19.8 ^{+0.2} _{-0.2}	20.8 ^{+0.1} _{-0.1}	1432.3/1459
ZTF21aaxleaq	280.350423	-17.636413	9350.42 ^{+0.54} _{-0.56}	0.33 ^{+0.01} _{-0.02}	91.9 ^{+3.3} _{-2.9}	19.4 ^{+0.1} _{-0.1}	20.2 ^{+0.1} _{-0.1}	2585.1/1748
ZTF19aamrjmu	280.734527	32.873077	8579.79 ^{+0.11} _{-0.11}	0.13 ^{+0.01} _{-0.01}	66.7 ^{+3.4} _{-3.0}	20.2 ^{+0.1} _{-0.1}	21.1 ^{+0.1} _{-0.1}	2799.5/1842
ZTF19abqueuo	280.805618	-16.299130	8731.02 ^{+0.86} _{-0.88}	0.37 ^{+0.16} _{-0.11}	91.1 ^{+24.8} _{-19.5}	18.0 ^{+0.5} _{-0.6}	19.3 ^{+0.5} _{-0.6}	937.6/824
ZTF20abaptby	280.809383	-8.669006	8991.91 ^{+0.16} _{-0.17}	0.19 ^{+0.04} _{-0.04}	16.3 ^{+1.6} _{-1.3}	18.8 ^{+0.2} _{-0.2}	21.0 ^{+0.2} _{-0.2}	996.1/592
ZTF22aauvkpi	280.821123	-9.539534	9798.18 ^{+0.32} _{-0.32}	0.44 ^{+0.02} _{-0.03}	41.8 ^{+1.9} _{-1.2}	18.1 ^{+0.1} _{-0.1}	19.2 ^{+0.1} _{-0.1}	1286.3/1135
ZTF21aciqmój	281.379089	-10.850293	9589.75 ^{+0.33} _{-0.33}	0.06 ^{+0.06} _{-0.04}	74.2 ^{+1.2} _{-0.8}	16.8 ^{+0.0} _{-0.0}	18.1 ^{+0.0} _{-0.0}	1035.1/1078
↑	↑	↑	9590.30 ^{+2.76} _{-3.22}	0.07 ^{+0.15} _{-0.15}	157.7 ^{+127.0} _{-51.2}	-0.441 ^{+0.262} _{-0.190}	-0.155 ^{+0.206} _{-0.164}	16.8 ^{+0.0} _{-0.0}	18.1 ^{+0.0} _{-0.0}	999.1/1076
ZTF22abfvhzh	281.467118	-10.898031	9834.97 ^{+0.19} _{-0.19}	0.15 ^{+0.04} _{-0.06}	13.5 ^{+0.9} _{-0.6}	18.6 ^{+0.2} _{-0.1}	19.8 ^{+0.1} _{-0.1}	1255.3/1044
ZTF19abijroe	281.724242	-12.913359	8696.45 ^{+0.17} _{-0.17}	0.24 ^{+0.03} _{-0.03}	25.9 ^{+2.6} _{-2.2}	20.4 ^{+0.2} _{-0.2}	...	483.8/377
ZTF19aavndrc	281.836917	-4.338119	8637.37 ^{+0.15} _{-0.16}	0.10 ^{+0.01} _{-0.01}	69.7 ^{+4.2} _{-3.8}	19.8 ^{+0.1} _{-0.1}	...	919.0/808
ZTF22aabpbdm	281.849345	-5.564412	9619.74 ^{+0.66} _{-0.67}	0.09 ^{+0.01} _{-0.01}	162.7 ^{+14.7} _{-13.0}	18.3 ^{+0.1} _{-0.1}	21.1 ^{+0.2} _{-0.2}	411.3/362
ZTF22aavemfz	282.068688	-13.867590	9795.18 ^{+0.31} _{-0.31}	0.12 ^{+0.02} _{-0.01}	77.0 ^{+6.9} _{-5.6}	20.4 ^{+0.1} _{-0.1}	...	143.6/161

Table 2 continued

Table 2 (continued)

ID	R.A. (J2000)	Decl. (J2000)	t_0 (HJD')	u_0	t_E	$\pi_{E,N}$	$\pi_{E,E}$	τ_s (mag)	g_s (mag)	$\chi^2/d.o.f$
ZTF19abjvsbc	282.108856	-26.677660	8713.71 $^{+0.05}_{-0.05}$	0.23 $^{+0.01}_{-0.01}$	20.4 $^{+0.7}_{-0.5}$	17.9 $^{+0.1}_{-0.0}$	18.5 $^{+0.1}_{-0.0}$	818.5/828
ZTF19aayqnmnp	282.308899	7.892137	8652.05 $^{+1.77}_{-1.92}$	0.26 $^{+0.16}_{-0.10}$	169.6 $^{+76.3}_{-52.4}$	21.5 $^{+0.6}_{-0.7}$	23.4 $^{+0.6}_{-0.7}$	1120.5/828
ZTF19abhznaj	283.104127	-10.176370	8691.70 $^{+0.01}_{-0.01}$	0.14 $^{+0.01}_{-0.01}$	4.0 $^{+0.1}_{-0.1}$	18.1 $^{+0.1}_{-0.0}$	18.9 $^{+0.1}_{-0.1}$	4145.1/1093
ZTF20abhmltf	283.251903	-19.851329	9043.34 $^{+0.52}_{-0.48}$	0.24 $^{+0.08}_{-0.06}$	55.3 $^{+12.6}_{-9.6}$	19.0 $^{+0.4}_{-0.4}$	19.7 $^{+0.4}_{-0.4}$	1585.6/1031
↑	↑	↑	9043.12 $^{+0.46}_{-0.44}$	0.39 $^{+0.04}_{-0.05}$	38.9 $^{+3.6}_{-2.1}$	0.043 $^{+0.113}_{-0.115}$	-0.925 $^{+0.101}_{-0.085}$	19.0 $^{+0.4}_{-0.4}$	19.7 $^{+0.4}_{-0.4}$	1524.7/1029
ZTF21aaxldzb	283.345900	-1.235099	9370.10 $^{+0.53}_{-0.54}$	0.27 $^{+0.01}_{-0.01}$	83.0 $^{+3.1}_{-2.8}$	19.2 $^{+0.1}_{-0.1}$...	1790.5/700
↑	↑	↑	9365.92 $^{+1.01}_{-1.25}$	0.18 $^{+0.06}_{-0.05}$	130.5 $^{+65.1}_{-31.9}$	0.158 $^{+0.230}_{-0.253}$	0.345 $^{+0.078}_{-0.119}$	19.2 $^{+0.1}_{-0.1}$...	1723.3/698
ZTF1853.4-0404	283.347360	-4.068832	9395.19 $^{+1.35}_{-1.40}$	0.61 $^{+0.12}_{-0.17}$	46.2 $^{+10.4}_{-5.2}$	19.2 $^{+0.5}_{-0.3}$	22.0 $^{+0.5}_{-0.3}$	947.6/761
ZTF1853.5-0415	283.366622	-4.251849	8291.84 $^{+0.56}_{-0.55}$	0.10 $^{+0.05}_{-0.04}$	65.5 $^{+23.3}_{-15.6}$	21.0 $^{+0.5}_{-0.5}$	23.8 $^{+0.5}_{-0.5}$	1067.9/887
ZTF19aaxsdqz	283.497178	-1.152234	8676.10 $^{+0.12}_{-0.11}$	0.18 $^{+0.01}_{-0.01}$	62.8 $^{+2.2}_{-1.8}$	19.0 $^{+0.1}_{-0.0}$	21.7 $^{+0.1}_{-0.1}$	850.9/513
↑	↑	↑	8675.64 $^{+0.15}_{-0.15}$	0.18 $^{+0.01}_{-0.01}$	63.6 $^{+3.5}_{-2.5}$	0.610 $^{+0.137}_{-0.129}$	0.109 $^{+0.140}_{-0.127}$	19.0 $^{+0.1}_{-0.1}$	21.7 $^{+0.1}_{-0.1}$	826.9/511
ZTF22aarwizr	283.668157	-3.352577	9787.56 $^{+0.43}_{-0.44}$	0.62 $^{+0.08}_{-0.10}$	36.5 $^{+4.4}_{-2.7}$	18.0 $^{+0.3}_{-0.2}$	21.3 $^{+0.3}_{-0.2}$	1437.7/1176
ZTF20abiogoc	283.857738	13.418495	9032.02 $^{+0.04}_{-0.04}$	0.03 $^{+0.01}_{-0.01}$	28.6 $^{+6.7}_{-4.7}$	22.2 $^{+0.3}_{-0.2}$...	559.8/520
ZTF19abcpeukt	283.871707	-10.752101	8691.42 $^{+0.02}_{-0.02}$	0.01 $^{+0.00}_{-0.00}$	143.7 $^{+9.7}_{-8.5}$	20.1 $^{+0.1}_{-0.1}$...	421.8/397
↑	↑	↑	8691.39 $^{+0.02}_{-0.02}$	0.01 $^{+0.00}_{-0.00}$	141.4 $^{+9.9}_{-8.7}$	0.119 $^{+0.035}_{-0.037}$	-0.170 $^{+0.025}_{-0.027}$	20.1 $^{+0.1}_{-0.1}$...	365.4/395
ZTF18abhxjmj	284.029165	13.152281	8249.23 $^{+0.21}_{-0.22}$	0.17 $^{+0.01}_{-0.01}$	46.6 $^{+1.9}_{-1.7}$	19.8 $^{+0.1}_{-0.1}$	21.3 $^{+0.1}_{-0.1}$	1406.7/1017
↑	↑	↑	8250.54 $^{+0.26}_{-0.25}$	0.09 $^{+0.02}_{-0.02}$	75.6 $^{+16.4}_{-9.7}$	-0.127 $^{+0.313}_{-0.435}$	-0.649 $^{+0.263}_{-0.160}$	19.8 $^{+0.1}_{-0.1}$	21.3 $^{+0.1}_{-0.1}$	1324.1/1015
ZTF1856.2-1010	284.049365	10.116731	8367.46 $^{+0.05}_{-0.05}$	0.05 $^{+0.01}_{-0.01}$	23.4 $^{+3.6}_{-3.2}$	21.3 $^{+0.2}_{-0.2}$	22.5 $^{+0.2}_{-0.2}$	2203.2/954
ZTF22aafvwx	284.061768	-1.168470	8352.42 $^{+0.05}_{-0.05}$	0.07 $^{+0.02}_{-0.02}$	20.9 $^{+4.4}_{-3.5}$	20.0 $^{+0.3}_{-0.3}$	21.6 $^{+0.3}_{-0.3}$	1127.8/918
ZTF21aawgkvn	284.551858	-8.580969	9679.21 $^{+0.16}_{-0.16}$	0.06 $^{+0.01}_{-0.01}$	86.6 $^{+6.9}_{-5.3}$	19.7 $^{+0.1}_{-0.1}$	20.5 $^{+0.1}_{-0.1}$	526.2/526
ZTF21aawgkvn	284.933398	-19.236220	9332.09 $^{+0.08}_{-0.08}$	0.24 $^{+0.01}_{-0.02}$	13.4 $^{+0.4}_{-0.3}$	17.9 $^{+0.1}_{-0.0}$	18.4 $^{+0.1}_{-0.0}$	1374.2/1090
ZTF19abjehsm	285.239280	-11.947921	8700.68 $^{+0.37}_{-0.39}$	0.53 $^{+0.18}_{-0.15}$	20.6 $^{+4.9}_{-3.2}$	19.0 $^{+0.5}_{-0.5}$	20.0 $^{+0.5}_{-0.5}$	1533.3/980
ZTF192.2+0001	285.539417	0.030083	8748.39 $^{+0.82}_{-0.81}$	0.47 $^{+0.04}_{-0.06}$	65.6 $^{+6.1}_{-3.7}$	19.2 $^{+0.2}_{-0.1}$	20.7 $^{+0.2}_{-0.1}$	1245.3/1003
ZTF18abmxlq	285.984027	-13.929453	8322.63 $^{+0.40}_{-0.40}$	0.40 $^{+0.05}_{-0.06}$	55.1 $^{+6.4}_{-3.8}$	18.0 $^{+0.2}_{-0.2}$	18.8 $^{+0.2}_{-0.2}$	1093.9/1090
ZTF22aafyxh	286.075804	0.374287	9640.89 $^{+0.70}_{-0.84}$	0.03 $^{+0.03}_{-0.02}$	35.3 $^{+3.8}_{-2.5}$	18.5 $^{+0.2}_{-0.2}$	20.2 $^{+0.2}_{-0.1}$	1293.9/617
ZTF21acqomnw	286.216530	-8.566820	9690.64 $^{+0.32}_{-0.32}$	0.29 $^{+0.01}_{-0.01}$	105.6 $^{+2.9}_{-2.9}$	15.5 $^{+0.1}_{-0.1}$	16.5 $^{+0.1}_{-0.1}$	944.1/992
ZTF21aaoeecs	286.303102	14.860000	9305.38 $^{+0.09}_{-0.09}$	0.10 $^{+0.01}_{-0.01}$	43.7 $^{+2.1}_{-2.0}$	18.8 $^{+0.1}_{-0.1}$...	1269.5/845
↑	↑	↑	9305.21 $^{+0.13}_{-0.14}$	0.02 $^{+0.01}_{-0.01}$	227.0 $^{+93.4}_{-78.3}$	-0.923 $^{+0.178}_{-0.188}$	0.200 $^{+0.048}_{-0.047}$	18.8 $^{+0.1}_{-0.1}$...	1239.4/843
ZTF20acpjzvw	286.411961	29.786491	9207.44 $^{+0.62}_{-0.65}$	0.43 $^{+0.08}_{-0.06}$	74.0 $^{+6.6}_{-6.6}$	19.2 $^{+0.2}_{-0.2}$	19.8 $^{+0.2}_{-0.2}$	5576.4/4374
↑	↑	↑	9215.12 $^{+1.28}_{-1.17}$	0.39 $^{+0.15}_{-0.10}$	68.9 $^{+16.8}_{-13.5}$	0.394 $^{+0.064}_{-0.056}$	0.134 $^{+0.099}_{-0.084}$	19.2 $^{+0.2}_{-0.2}$	19.8 $^{+0.2}_{-0.2}$	5486.0/4372
ZTF19abjtzvc	286.468603	-9.741298	8709.78 $^{+0.58}_{-0.57}$	0.12 $^{+0.05}_{-0.04}$	170.1 $^{+69.6}_{-43.8}$	21.3 $^{+0.5}_{-0.4}$...	645.9/500

Table 2 continued

Table 2 (continued)

ID	R.A. (J2000)	Decl. (J2000)	t_0 (HJD ^a)	u_0	t_E	$\pi_{E,N}$	$\pi_{E,E}$	τ_s (mag)	g_s (mag)	$\chi^2/d.o.f$
ZTF22abazvnk	286.499515	10.185071	9818.14 ^{+0.21} _{-0.22}	0.08 ^{+0.02} _{-0.02}	62.9 ^{+11.8} _{-9.4}	21.2 ^{+0.3} _{-0.2}	...	769.8/628
ZTF22aaqxhng	286.502828	-12.820282	9762.80 ^{+0.04} _{-0.04}	0.22 ^{+0.02} _{-0.02}	10.7 ^{+0.7} _{-0.6}	17.7 ^{+0.1} _{-0.1}	18.8 ^{+0.1} _{-0.1}	2328.4/1014
ZTF22abambyf	286.714173	3.314354	9849.39 ^{+0.17} _{-0.17}	0.15 ^{+0.01} _{-0.01}	59.6 ^{+2.3} _{-2.2}	18.4 ^{+0.1} _{-0.1}	20.0 ^{+0.1} _{-0.1}	1939.6/1101
↑	↑	↑	9848.76 ^{+0.22} _{-0.23}	0.12 ^{+0.02} _{-0.02}	73.0 ^{+14.3} _{-9.2}	0.502 ^{+0.138} _{-0.175}	-0.164 ^{+0.032} _{-0.034}	18.4 ^{+0.1} _{-0.1}	20.0 ^{+0.1} _{-0.1}	1905.8/1099
ZTF21aahtzmf	286.882512	-5.330409	9268.53 ^{+0.16} _{-0.16}	0.16 ^{+0.01} _{-0.01}	38.3 ^{+1.2} _{-0.9}	18.1 ^{+0.1} _{-0.1}	19.0 ^{+0.1} _{-0.1}	1648.5/1255
ZTF22abcjuat ^a	286.983580	27.629135	9844.44 ^{+0.03} _{-0.03}	0.000024 ^{+0.000046} _{-0.000015}	23146.4 ^{+27467.7} _{-13821.3}	27.5 ^{+1.0} _{-1.0}	28.3 ^{+1.0} _{-1.2}	3430.8/1248
ZTF20acutkqi	287.321741	14.969378	9204.29 ^{+0.67} _{-0.67}	0.15 ^{+0.02} _{-0.02}	104.5 ^{+9.0} _{-7.9}	19.8 ^{+0.1} _{-0.1}	21.6 ^{+0.2} _{-0.2}	2319.3/1178
ZTF22abifztl	287.510986	-9.706967	9857.54 ^{+0.15} _{-0.15}	0.21 ^{+0.04} _{-0.04}	20.4 ^{+3.6} _{-2.3}	20.1 ^{+0.3} _{-0.2}	21.0 ^{+0.3} _{-0.2}	889.5/712
ZTF19aaocwvc	287.557245	12.559859	8580.96 ^{+0.53} _{-0.52}	0.12 ^{+0.03} _{-0.03}	81.1 ^{+14.4} _{-11.8}	20.8 ^{+0.3} _{-0.3}	22.7 ^{+0.3} _{-0.3}	997.5/823
ZTF19aaopcxy	287.969450	3.949465	8551.34 ^{+0.85} _{-0.84}	0.21 ^{+0.08} _{-0.07}	108.8 ^{+16.4} _{-12.1}	20.0 ^{+0.3} _{-0.3}	...	979.9/716
↑	↑	↑	8546.10 ^{+1.54} _{-1.74}	0.03 ^{+0.10} _{-0.06}	160.8 ^{+66.7} _{-51.5}	-0.244 ^{+0.039} _{-0.044}	0.218 ^{+0.091} _{-0.064}	20.0 ^{+0.3} _{-0.3}	...	949.1/714
ZTF22aaajlxl	288.013245	-13.906334	9713.93 ^{+0.09} _{-0.09}	0.03 ^{+0.00} _{-0.00}	39.1 ^{+2.7} _{-2.2}	20.3 ^{+0.1} _{-0.1}	21.2 ^{+0.1} _{-0.1}	711.7/605
ZTF21abiqqzh	288.427009	4.915432	9460.94 ^{+0.66} _{-0.65}	0.21 ^{+0.02} _{-0.02}	203.1 ^{+14.4} _{-13.0}	19.8 ^{+0.1} _{-0.1}	21.9 ^{+0.1} _{-0.1}	1790.7/1088
ZTF21aaymbrh	289.161402	5.321489	9346.63 ^{+0.36} _{-0.36}	0.13 ^{+0.02} _{-0.02}	76.0 ^{+8.2} _{-6.6}	20.8 ^{+0.2} _{-0.1}	...	574.6/438
ZTF22aaalsar	289.730054	3.728906	9778.77 ^{+0.27} _{-0.28}	0.09 ^{+0.01} _{-0.01}	143.3 ^{+19.0} _{-16.2}	20.8 ^{+0.2} _{-0.2}	22.1 ^{+0.2} _{-0.2}	1012.1/621
↑	↑	↑	9778.39 ^{+0.28} _{-0.28}	0.18 ^{+0.02} _{-0.02}	79.3 ^{+6.5} _{-5.2}	0.066 ^{+0.055} _{-0.055}	-0.325 ^{+0.054} _{-0.049}	20.8 ^{+0.2} _{-0.2}	22.1 ^{+0.2} _{-0.2}	978.7/619
ZTF20acbmtdw	289.939298	23.204269	9150.54 ^{+1.03} _{-0.98}	0.26 ^{+0.07} _{-0.07}	85.5 ^{+18.3} _{-12.3}	20.7 ^{+0.4} _{-0.3}	22.5 ^{+0.4} _{-0.3}	850.5/508
↑	↑	↑	9148.79 ^{+1.00} _{-1.09}	0.23 ^{+0.09} _{-0.09}	90.3 ^{+46.1} _{-19.6}	-0.271 ^{+0.192} _{-0.155}	-0.123 ^{+0.061} _{-0.063}	20.7 ^{+0.4} _{-0.3}	22.5 ^{+0.4} _{-0.3}	829.5/506
ZTF20aavmhsg	290.016403	37.434802	8982.94 ^{+0.12} _{-0.12}	0.12 ^{+0.01} _{-0.01}	46.0 ^{+4.2} _{-3.7}	19.8 ^{+0.1} _{-0.1}	20.9 ^{+0.1} _{-0.1}	1965.8/1296
↑	↑	↑	8983.15 ^{+0.13} _{-0.13}	0.09 ^{+0.01} _{-0.01}	56.5 ^{+6.6} _{-5.4}	0.026 ^{+0.106} _{-0.081}	-0.544 ^{+0.079} _{-0.088}	19.8 ^{+0.1} _{-0.1}	20.9 ^{+0.1} _{-0.1}	1933.2/1294
ZTF1921.4+2442	290.338814	24.704692	9144.47 ^{+0.95} _{-0.94}	0.35 ^{+0.04} _{-0.05}	66.8 ^{+5.9} _{-4.2}	20.6 ^{+0.2} _{-0.2}	21.8 ^{+0.2} _{-0.2}	1821.6/1347
ZTF18abaqxrt	290.617206	1.706493	8302.05 ^{+0.20} _{-0.20}	0.61 ^{+0.06} _{-0.07}	33.2 ^{+2.5} _{-2.0}	14.7 ^{+0.2} _{-0.2}	16.3 ^{+0.2} _{-0.2}	1786.9/1106
↑	↑	↑	8303.01 ^{+0.25} _{-0.25}	0.61 ^{+0.07} _{-0.09}	33.3 ^{+4.0} _{-2.5}	-1.316 ^{+0.246} _{-0.258}	-0.512 ^{+0.209} _{-0.194}	14.7 ^{+0.2} _{-0.2}	16.3 ^{+0.2} _{-0.2}	1731.8/1104
ZTF20abkyuyk	290.832471	23.773102	9085.08 ^{+0.10} _{-0.10}	0.41 ^{+0.02} _{-0.03}	36.3 ^{+1.6} _{-1.3}	17.7 ^{+0.1} _{-0.1}	19.1 ^{+0.1} _{-0.1}	1731.4/1616
↑	↑	↑	9085.67 ^{+0.21} _{-0.19}	0.28 ^{+0.07} _{-0.06}	53.8 ^{+16.6} _{-10.1}	0.677 ^{+0.268} _{-0.327}	0.738 ^{+0.152} _{-0.191}	17.7 ^{+0.1} _{-0.1}	19.1 ^{+0.1} _{-0.1}	1703.4/1614
ZTF20acjzftp	291.937805	-0.336323	9195.88 ^{+0.74} _{-0.71}	0.37 ^{+0.01} _{-0.01}	79.7 ^{+1.9} _{-1.8}	19.0 ^{+0.1} _{-0.0}	19.7 ^{+0.1} _{-0.0}	1816.5/1106
↑	↑	↑	9187.27 ^{+2.14} _{-2.09}	0.17 ^{+0.06} _{-0.04}	167.4 ^{+54.2} _{-41.5}	0.038 ^{+0.107} _{-0.127}	-0.287 ^{+0.045} _{-0.044}	19.0 ^{+0.1} _{-0.0}	19.7 ^{+0.1} _{-0.0}	1749.4/1104
ZTF1928.7+3039	292.175983	30.664607	8369.94 ^{+0.33} _{-0.35}	0.09 ^{+0.03} _{-0.03}	37.3 ^{+10.4} _{-6.7}	21.7 ^{+0.4} _{-0.4}	...	347.4/313
ZTF20abmxjsq	293.061918	25.482549	9051.43 ^{+0.46} _{-0.46}	0.22 ^{+0.08} _{-0.08}	75.7 ^{+19.1} _{-15.0}	21.0 ^{+0.4} _{-0.4}	22.8 ^{+0.4} _{-0.4}	1425.8/1025

Table 2 continued

^a A potential one-lens two-source event.

Table 2 (continued)

ID	R.A (J2000)	Decl. (J2000)	t_0 (HJD')	u_0	t_E	$\pi_{E,N}$	$\pi_{E,E}$	τ_s (mag)	g_s (mag)	$\chi^2/d.o.f$
ZTF21abotlit	293.757264	32.016097	9446.67 ^{+0.29} _{-0.30}	0.28 ^{+0.01} _{-0.01}	76.2 ^{+2.5} _{-2.1}	19.4 ^{+0.1} _{-0.1}	20.1 ^{+0.1} _{-0.1}	1573.0/1130
↑	↑	↑	9442.89 ^{+0.41} _{-0.43}	0.22 ^{+0.04} _{-0.04}	94.1 ^{+14.6} _{-10.7}	0.400 ^{+0.044} _{-0.043}	-0.318 ^{+0.056} _{-0.056}	19.4 ^{+0.1} _{-0.1}	20.1 ^{+0.1} _{-0.1}	1275.6/1128
ZTF21abouknq	294.286666	13.095785	9458.03 ^{+1.25} _{-1.25}	0.48 ^{+0.04} _{-0.06}	135.1 ^{+11.6} _{-7.2}	19.2 ^{+0.2} _{-0.1}	20.3 ^{+0.2} _{-0.1}	1263.5/1112
ZTF20achpgdp	294.817816	-5.055385	9150.50 ^{+0.32} _{-0.33}	0.28 ^{+0.01} _{-0.02}	70.6 ^{+2.7} _{-2.5}	19.9 ^{+0.1} _{-0.1}	21.0 ^{+0.1} _{-0.1}	2087.5/1165
↑	↑	↑	9147.36 ^{+0.33} _{-0.33}	0.17 ^{+0.03} _{-0.02}	89.2 ^{+10.0} _{-9.3}	-0.468 ^{+0.113} _{-0.104}	-0.332 ^{+0.053} _{-0.064}	19.9 ^{+0.1} _{-0.1}	21.0 ^{+0.1} _{-0.1}	1812.2/1163
ZTF20abrtvzb	294.844573	39.178278	9089.21 ^{+0.27} _{-0.27}	0.11 ^{+0.03} _{-0.03}	64.0 ^{+14.8} _{-10.9}	21.4 ^{+0.3} _{-0.3}	22.2 ^{+0.3} _{-0.3}	1698.4/1271
ZTF22aanukpr	295.997220	18.506507	9760.13 ^{+0.09} _{-0.09}	0.09 ^{+0.01} _{-0.01}	44.0 ^{+2.7} _{-2.5}	19.3 ^{+0.1} _{-0.1}	20.5 ^{+0.1} _{-0.1}	3175.1/1230
ZTF22abgwuap	297.603439	5.236071	9877.09 ^{+0.04} _{-0.04}	0.15 ^{+0.00} _{-0.00}	28.4 ^{+0.3} _{-0.2}	17.9 ^{+0.0} _{-0.0}	18.4 ^{+0.0} _{-0.0}	2011.5/1240
↑	↑	↑	9877.27 ^{+0.06} _{-0.06}	0.15 ^{+0.01} _{-0.01}	31.0 ^{+1.9} _{-1.1}	1.880 ^{+0.318} _{-0.316}	-0.082 ^{+0.079} _{-0.083}	17.9 ^{+0.0} _{-0.0}	18.4 ^{+0.0} _{-0.0}	1971.5/1238
ZTF19aavisrq	297.706148	34.637372	8651.81 ^{+0.02} _{-0.02}	0.02 ^{+0.00} _{-0.00}	93.8 ^{+4.7} _{-4.3}	20.6 ^{+0.1} _{-0.1}	21.6 ^{+0.1} _{-0.1}	1677.2/1524
↑	↑	↑	8651.83 ^{+0.02} _{-0.02}	0.02 ^{+0.00} _{-0.00}	103.6 ^{+8.1} _{-6.6}	-0.064 ^{+0.043} _{-0.045}	-0.099 ^{+0.065} _{-0.053}	20.6 ^{+0.1} _{-0.1}	21.6 ^{+0.1} _{-0.1}	1656.2/1522
ZTF20abohkdo	298.050409	26.993506	9061.61 ^{+0.13} _{-0.13}	0.10 ^{+0.02} _{-0.02}	44.5 ^{+8.1} _{-6.6}	21.7 ^{+0.2} _{-0.2}	23.9 ^{+0.2} _{-0.2}	1944.1/1306
ZTF19acaagd	298.683905	5.402621	8761.98 ^{+0.05} _{-0.05}	0.02 ^{+0.00} _{-0.00}	101.6 ^{+7.2} _{-6.4}	21.6 ^{+0.1} _{-0.1}	22.4 ^{+0.1} _{-0.1}	3773.8/1808
ZTF18abtopdh	299.292602	35.443630	8367.90 ^{+0.04} _{-0.04}	0.06 ^{+0.01} _{-0.01}	23.5 ^{+1.5} _{-1.4}	20.8 ^{+0.1} _{-0.1}	22.6 ^{+0.1} _{-0.1}	2170.9/1040
ZTF20abbynqb	301.318169	55.322594	9046.50 ^{+0.16} _{-0.16}	0.36 ^{+0.03} _{-0.03}	54.8 ^{+3.0} _{-2.9}	17.6 ^{+0.1} _{-0.1}	18.7 ^{+0.1} _{-0.1}	1657.2/1262
↑	↑	↑	9045.29 ^{+0.20} _{-0.19}	0.68 ^{+0.04} _{-0.06}	33.4 ^{+2.4} _{-1.4}	0.511 ^{+0.053} _{-0.055}	-0.423 ^{+0.128} _{-0.116}	17.6 ^{+0.1} _{-0.1}	18.7 ^{+0.1} _{-0.1}	1502.4/1260
ZTF20abxwvnr	301.549799	35.631697	9117.28 ^{+0.01} _{-0.01}	0.01 ^{+0.00} _{-0.00}	158.3 ^{+14.0} _{-12.0}	22.0 ^{+0.1} _{-0.1}	...	797.8/651
↑	↑	↑	9117.32 ^{+0.02} _{-0.02}	0.01 ^{+0.00} _{-0.00}	167.7 ^{+51.2} _{-32.0}	0.243 ^{+0.037} _{-0.040}	0.273 ^{+0.066} _{-0.057}	22.0 ^{+0.1} _{-0.1}	...	728.9/649
ZTF18abnbsmr	307.149387	22.830473	8363.13 ^{+0.19} _{-0.19}	0.29 ^{+0.04} _{-0.03}	38.9 ^{+3.0} _{-2.9}	19.0 ^{+0.1} _{-0.2}	19.6 ^{+0.1} _{-0.2}	2269.0/1463
ZTF21abqhbuh	307.424553	31.295265	9520.45 ^{+0.02} _{-0.02}	0.04 ^{+0.00} _{-0.00}	60.9 ^{+0.6} _{-0.6}	15.8 ^{+0.0} _{-0.0}	17.4 ^{+0.0} _{-0.0}	3211.6/1347
↑	↑	↑	9520.32 ^{+0.02} _{-0.02}	0.04 ^{+0.00} _{-0.00}	57.8 ^{+0.8} _{-0.6}	-0.205 ^{+0.028} _{-0.027}	-0.042 ^{+0.011} _{-0.012}	15.8 ^{+0.0} _{-0.0}	17.4 ^{+0.0} _{-0.0}	2915.7/1345
ZTF19aavnrtq	309.034118	32.720917	8722.29 ^{+0.31} _{-0.32}	0.61 ^{+0.01} _{-0.02}	80.2 ^{+1.6} _{-0.9}	17.2 ^{+0.1} _{-0.0}	19.3 ^{+0.1} _{-0.0}	3560.9/1750
↑	↑	↑	8721.05 ^{+0.59} _{-0.58}	0.53 ^{+0.07} _{-0.09}	106.6 ^{+21.7} _{-13.2}	0.236 ^{+0.044} _{-0.042}	0.062 ^{+0.044} _{-0.048}	17.2 ^{+0.1} _{-0.0}	19.3 ^{+0.1} _{-0.0}	3524.2/1748
ZTF22aagdkla	311.543933	51.684673	9726.41 ^{+0.07} _{-0.07}	0.27 ^{+0.01} _{-0.01}	45.3 ^{+0.8} _{-0.5}	15.9 ^{+0.0} _{-0.0}	17.0 ^{+0.0} _{-0.0}	1615.7/1386
↑	↑	↑	9727.51 ^{+0.13} _{-0.11}	0.14 ^{+0.02} _{-0.02}	81.6 ^{+13.2} _{-9.3}	-0.655 ^{+0.078} _{-0.064}	0.033 ^{+0.048} _{-0.054}	15.9 ^{+0.0} _{-0.0}	17.0 ^{+0.0} _{-0.0}	1229.3/1384
ZTF2050.9+2747	312.717949	27.783574	9860.33 ^{+0.49} _{-0.49}	0.39 ^{+0.18} _{-0.12}	42.5 ^{+12.2} _{-9.2}	19.5 ^{+0.5} _{-0.6}	20.3 ^{+0.5} _{-0.6}	1986.8/1292
ZTF19acptvtn	315.713353	32.811690	8777.40 ^{+0.16} _{-0.16}	0.19 ^{+0.01} _{-0.01}	38.0 ^{+1.8} _{-1.7}	20.3 ^{+0.1} _{-0.1}	20.5 ^{+0.1} _{-0.1}	1768.6/827
ZTF19abftuld	318.263354	43.337654	8728.75 ^{+0.13} _{-0.13}	0.19 ^{+0.02} _{-0.02}	104.5 ^{+10.2} _{-8.6}	20.4 ^{+0.1} _{-0.1}	21.5 ^{+0.1} _{-0.1}	1904.4/1367
↑	↑	↑	8729.52 ^{+0.19} _{-0.15}	0.39 ^{+0.02} _{-0.03}	54.5 ^{+4.2} _{-2.3}	-0.507 ^{+0.053} _{-0.040}	-0.251 ^{+0.148} _{-0.078}	20.4 ^{+0.1} _{-0.1}	21.5 ^{+0.1} _{-0.1}	1749.9/1365
ZTF22abmqxzi	318.845306	50.028538	9873.93 ^{+0.86} _{-0.81}	0.10 ^{+0.07} _{-0.04}	103.5 ^{+53.3} _{-33.2}	21.9 ^{+0.6} _{-0.6}	23.9 ^{+0.6} _{-0.6}	2463.3/1933
ZTF21abtlxpr	321.374546	46.419130	9469.22 ^{+0.03} _{-0.03}	0.02 ^{+0.00} _{-0.00}	128.5 ^{+6.3} _{-5.8}	20.2 ^{+0.1} _{-0.1}	21.5 ^{+0.1} _{-0.1}	2496.8/1600

Table 2 continued

Table 2 (continued)

ID	R.A. (J2000)	Decl. (J2000)	t_0 (HJD $'$)	u_0	t_E	$\pi_{E,N}$	$\pi_{E,E}$	τ_s (mag)	g_s (mag)	$\chi^2/\text{d.o.f}$
\uparrow	\uparrow	\uparrow	$9469.25^{+0.03}_{-0.03}$	$0.03^{+0.00}_{-0.00}$	$81.2^{+2.7}_{-2.4}$	$-0.256^{+0.017}_{-0.016}$	$-0.263^{+0.013}_{-0.012}$	$20.2^{+0.1}_{-0.1}$	$21.5^{+0.1}_{-0.1}$	2268.5/1598
ZTF20abvwhlb	324.577344	48.479249	$9090.34^{+0.02}_{-0.02}$	$0.22^{+0.01}_{-0.01}$	$8.8^{+0.4}_{-0.3}$	$18.8^{+0.1}_{-0.1}$	$19.7^{+0.1}_{-0.1}$	3253.6/1950
ZTF18aaztjyd	326.173128	59.377902	$8290.09^{+0.20}_{-0.21}$	$0.13^{+0.02}_{-0.02}$	$71.7^{+9.6}_{-7.8}$	$21.1^{+0.2}_{-0.2}$	$22.5^{+0.2}_{-0.2}$	749.9/590
ZTF18aayhjoe	329.192964	54.098564	$8278.56^{+0.27}_{-0.27}$	$0.50^{+0.03}_{-0.04}$	$27.9^{+1.7}_{-1.1}$	$19.8^{+0.1}_{-0.1}$	$21.2^{+0.1}_{-0.1}$	2650.0/1867
ZTF18adadlqt	349.022798	52.084154	$9432.96^{+0.04}_{-0.04}$	$0.41^{+0.09}_{-0.08}$	$6.6^{+0.7}_{-0.6}$	$15.3^{+0.3}_{-0.3}$	$15.8^{+0.3}_{-0.3}$	2255.5/1347

Table 3. List of Possible Microlensing Events in ZTF DR17 with MCMC Parameters

ID	R.A (J2000)	Decl. (J2000)	t_0 (HJD ^a)	u_0	t_E	$\pi_{E,N}$	$\pi_{E,E}$	r_s (mag)	g_s (mag)	$\chi^2/\text{d.o.f}$
ZTF19abfrdeg	17.324452	54.493693	8307.49 ^{+0.69} _{-0.71}	0.21 ^{+0.12} _{-0.09}	37.1 ^{+19.7} _{-10.1}	21.4 ^{+0.7} _{-0.6}	22.7 ^{+0.7} _{-0.6}	349.9/189
ZTF0139.2+5403	24.793413	54.063825	8296.18 ^{+0.21} _{-0.20}	0.03 ^{+0.54} _{-0.02}	24.3 ^{+5.4} _{-4.3}	21.1 ^{+0.3} _{-0.3}	23.1 ^{+0.2} _{-0.3}	1441.7/613
ZTF18acdyfuk	37.180587	38.914464	8441.71 ^{+0.68} _{-0.66}	0.23 ^{+0.03} _{-0.03}	45.4 ^{+4.9} _{-4.1}	21.0 ^{+0.2} _{-0.2}	21.0 ^{+0.2} _{-0.2}	176.8/106
ZTF19aabuqn	48.694297	62.343460	8506.15 ^{+0.44} _{-0.43}	0.22 ^{+0.10} _{-0.07}	45.2 ^{+14.0} _{-10.2}	20.1 ^{+0.5} _{-0.5}	21.6 ^{+0.4} _{-0.5}	656.3/270
ZTF18acbvsvfm	55.872634	39.674278	8418.93 ^{+1.64} _{-1.86}	0.14 ^{+0.03} _{-0.03}	91.6 ^{+18.5} _{-12.0}	21.1 ^{+0.3} _{-0.2}	21.4 ^{+0.3} _{-0.2}	103.3/61
ZTF0354.4+2948	58.590351	29.802082	8450.39 ^{+2.42} _{-2.53}	0.16 ^{+0.06} _{-0.06}	206.7 ^{+85.0} _{-42.1}	20.9 ^{+0.5} _{-0.4}	...	207.9/69
ZTF20actffyp	62.413830	44.068973	9241.47 ^{+1.16} _{-1.18}	0.46 ^{+0.19} _{-0.12}	115.1 ^{+25.8} _{-22.7}	19.6 ^{+0.5} _{-0.6}	20.5 ^{+0.5} _{-0.6}	1687.0/1097
ZTF20aacghde	66.840857	17.220539	8860.68 ^{+0.79} _{-0.77}	0.46 ^{+0.12} _{-0.15}	19.2 ^{+5.7} _{-2.8}	20.1 ^{+0.6} _{-0.4}	21.1 ^{+0.6} _{-0.4}	985.3/403
ZTF0545.5+5952	86.376567	59.880607	8840.60 ^{+0.35} _{-0.36}	0.32 ^{+0.05} _{-0.06}	29.0 ^{+4.3} _{-2.8}	20.3 ^{+0.3} _{-0.2}	20.9 ^{+0.3} _{-0.2}	511.4/269
ZTF19abpangr	90.818465	53.608017	8698.10 ^{+2.71} _{-2.24}	0.04 ^{+0.01} _{-0.02}	109.2 ^{+20.2} _{-13.7}	21.0 ^{+0.3} _{-0.3}	22.2 ^{+0.3} _{-0.3}	1048.0/568
ZTF20acvbjbw	100.236340	47.608269	9191.09 ^{+0.44} _{-0.45}	0.45 ^{+0.11} _{-0.11}	31.0 ^{+6.7} _{-4.3}	20.6 ^{+0.4} _{-0.4}	21.1 ^{+0.4} _{-0.4}	1687.0/858
ZTF20abwiild	108.819464	16.029165	9089.08 ^{+0.41} _{-0.43}	0.11 ^{+0.01} _{-0.01}	127.3 ^{+7.8} _{-6.8}	20.3 ^{+0.1} _{-0.1}	20.9 ^{+0.1} _{-0.1}	1335.0/610
ZTF170.4-2209	255.107688	-22.149985	8667.65 ^{+0.04} _{-0.04}	0.02 ^{+0.01} _{-0.01}	12.3 ^{+4.4} _{-2.7}	22.0 ^{+0.4} _{-0.3}	21.8 ^{+0.4} _{-0.3}	786.8/325
ZTF22aakboak ^a	266.033334	-16.731047	9718.29 ^{+0.29} _{-0.16}	0.000024 ^{+0.000417} _{-0.000023}	22662.7 ^{+872921.3} _{-21381.0}	28.3 ^{+4.0} _{-3.1}	...	131.7/119
ZTF22abcfiaq	267.861895	-12.370507	9843.67 ^{+0.93} _{-0.91}	0.58 ^{+0.04} _{-0.06}	58.1 ^{+4.1} _{-2.7}	19.3 ^{+0.2} _{-0.1}	20.9 ^{+0.2} _{-0.1}	1190.4/781
ZTF1752.5-2006	268.131417	-20.102409	9433.10 ^{+0.61} _{-0.48}	0.24 ^{+0.07} _{-0.08}	20.2 ^{+4.8} _{-2.9}	19.9 ^{+0.4} _{-0.3}	...	412.4/282
ZTF1756.4-1615	269.099954	-16.256962	8612.39 ^{+151.07} _{-4.83}	0.69 ^{+0.36} _{-0.17}	131.2 ^{+44.7} _{-14.9}	18.6 ^{+0.5} _{-0.3}	20.3 ^{+0.5} _{-0.3}	403.2/481
ZTF21aaygooe	269.206782	-18.039390	9355.48 ^{+1.33} _{-1.45}	0.30 ^{+0.04} _{-0.06}	48.7 ^{+7.5} _{-4.5}	18.8 ^{+0.3} _{-0.2}	20.7 ^{+0.3} _{-0.2}	183.1/195
ZTF22abcfjfp	271.174005	-18.458122	9823.26 ^{+0.27} _{-0.25}	0.40 ^{+0.03} _{-0.05}	14.1 ^{+1.3} _{-0.8}	19.0 ^{+0.2} _{-0.1}	...	592.0/451
ZTF18ablrdec	271.439134	-12.014536	8353.77 ^{+0.46} _{-0.50}	0.17 ^{+0.02} _{-0.03}	50.9 ^{+5.0} _{-3.9}	20.1 ^{+0.2} _{-0.1}	22.3 ^{+0.2} _{-0.1}	445.1/357
ZTF19aawehkq	271.794671	-14.315653	8634.69 ^{+1.27} _{-1.24}	0.11 ^{+0.06} _{-0.04}	91.8 ^{+38.3} _{-23.0}	21.5 ^{+0.5} _{-0.5}	22.9 ^{+0.5} _{-0.5}	733.5/577
ZTF18ablrkjk	271.850478	-10.314385	8260.99 ^{+1.15} _{-1.19}	0.12 ^{+0.07} _{-0.05}	111.6 ^{+54.5} _{-34.4}	21.9 ^{+0.6} _{-0.6}	...	335.2/256
ZTF188.2+2207	272.062138	22.128554	9168.08 ^{+0.49} _{-0.49}	0.18 ^{+0.03} _{-0.04}	42.8 ^{+9.0} _{-5.5}	20.9 ^{+0.3} _{-0.2}	21.2 ^{+0.3} _{-0.2}	411.3/239
ZTF18abaphdu	275.646637	-0.018457	8259.21 ^{+0.11} _{-0.12}	0.14 ^{+0.03} _{-0.03}	15.4 ^{+3.4} _{-2.3}	20.9 ^{+0.3} _{-0.2}	...	186.3/114
ZTF18abstrimp	275.878861	-7.332711	8394.80 ^{+8.12} _{-11.22}	0.17 ^{+0.16} _{-0.12}	65.8 ^{+23.3} _{-9.8}	19.6 ^{+0.9} _{-0.9}	...	646.3/551
ZTF1829.7-1829	277.436171	-18.499529	8681.57 ^{+1.23} _{-1.27}	0.07 ^{+0.17} _{-0.05}	322.4 ^{+912.9} _{-207.5}	21.7 ^{+1.6} _{-1.5}	23.1 ^{+1.6} _{-1.5}	298.2/344
ZTF1836.3+0354	279.083032	3.904392	9783.47 ^{+0.85} _{-0.84}	0.27 ^{+0.09} _{-0.11}	66.5 ^{+31.2} _{-12.8}	21.3 ^{+0.7} _{-0.4}	...	212.4/166

Table 3 continued

^a A potential one-lens two-source event.

Table 3 (continued)

ID	R-A (J2000)	Decl. (J2000)	t_0 (HJD')	u_0	t_E	$\pi_{E,N}$	$\pi_{E,E}$	τ_s (mag)	g_s (mag)	$\chi^2/d.o.f$
ZTF1837.0-1723	279.243098	-17.390309	9505.52 ^{+0.75} _{-0.66}	0.06 ^{+0.08} _{-0.04}	86.8 ^{+16.6} _{-14.9}	21.1 ^{+0.3} _{-0.4}	22.4 ^{+0.3} _{-0.4}	617.1/693
ZTF18abqbeqv	279.578746	7.837890	8383.77 ^{+1.34} _{-1.34}	0.94 ^{+0.17} _{-0.20}	57.0 ^{+9.4} _{-5.8}	17.2 ^{+0.5} _{-0.4}	18.3 ^{+0.5} _{-0.4}	1530.0/1250
ZTF20aameaz	280.052833	-2.370286	8892.89 ^{+0.32} _{-0.28}	0.05 ^{+0.01} _{-0.01}	52.6 ^{+10.6} _{-7.1}	20.3 ^{+0.3} _{-0.2}	...	578.8/498
ZTF1844.0-1439	281.003859	-14.660370	8963.52 ^{+3.92} _{-4.46}	0.56 ^{+0.06} _{-0.09}	105.9 ^{+13.5} _{-7.1}	18.8 ^{+0.3} _{-0.2}	20.1 ^{+0.3} _{-0.2}	1036.2/885
ZTF21aaygflq	281.016726	23.606018	9365.79 ^{+0.94} _{-0.95}	0.06 ^{+0.02} _{-0.02}	521.9 ^{+264.0} _{-136.7}	22.8 ^{+0.5} _{-0.4}	23.5 ^{+0.5} _{-0.4}	1426.4/886
ZTF22aapnaje	281.050554	-13.763612	9770.54 ^{+0.31} _{-0.31}	0.22 ^{+0.09} _{-0.06}	27.9 ^{+4.9} _{-4.4}	19.7 ^{+0.4} _{-0.4}	21.0 ^{+0.4} _{-0.4}	1379.3/1035
ZTF22aaajzoi	281.382698	2.182179	9673.61 ^{+1.04} _{-1.00}	0.43 ^{+0.13} _{-0.09}	98.5 ^{+16.3} _{-15.6}	19.1 ^{+0.3} _{-0.4}	22.6 ^{+0.4} _{-0.4}	1608.1/1054
ZTF1850.2+1007	282.560378	10.131160	8353.02 ^{+0.34} _{-0.37}	0.20 ^{+0.04} _{-0.04}	15.8 ^{+2.4} _{-1.7}	20.8 ^{+0.3} _{-0.2}	...	95.1/94
ZTF22aaojnic	283.673476	-12.068404	9746.19 ^{+0.16} _{-0.14}	0.08 ^{+0.04} _{-0.04}	27.7 ^{+12.9} _{-6.3}	21.1 ^{+0.6} _{-0.4}	...	253.6/257
ZTF1857.6-0936	284.403526	-9.606916	9558.65 ^{+6.98} _{-9.02}	0.15 ^{+0.08} _{-0.08}	222.4 ^{+151.4} _{-50.8}	21.0 ^{+0.9} _{-0.5}	21.7 ^{+0.9} _{-0.5}	497.0/402
ZTF20aawxugf	284.869767	-18.107711	8968.83 ^{+1.19} _{-1.26}	0.21 ^{+0.08} _{-0.05}	106.3 ^{+26.5} _{-23.5}	20.0 ^{+0.4} _{-0.5}	20.7 ^{+0.4} _{-0.5}	1542.4/1084
ZTF18absjezs	285.338355	-11.404525	8369.91 ^{+0.47} _{-0.46}	0.29 ^{+0.04} _{-0.04}	47.2 ^{+4.1} _{-3.5}	19.7 ^{+0.2} _{-0.2}	20.7 ^{+0.2} _{-0.2}	1244.8/814
ZTF20aanlcqv	285.890400	-0.967836	8894.39 ^{+2.73} _{-2.47}	0.21 ^{+0.05} _{-0.06}	171.9 ^{+38.3} _{-23.0}	20.8 ^{+0.4} _{-0.3}	...	572.6/445
ZTF20acgkxzp	286.127350	10.900394	9134.23 ^{+1.35} _{-1.27}	0.46 ^{+0.05} _{-0.08}	49.0 ^{+6.5} _{-3.9}	20.5 ^{+0.3} _{-0.2}	...	873.0/705
ZTF20acpjazv	286.411945	29.786498	9207.42 ^{+0.62} _{-0.64}	0.43 ^{+0.08} _{-0.06}	74.0 ^{+6.4} _{-6.6}	19.2 ^{+0.2} _{-0.2}	19.8 ^{+0.2} _{-0.2}	5576.4/4374
ZTF18aazluqp	286.860549	3.929120	8283.89 ^{+0.32} _{-0.32}	0.15 ^{+0.01} _{-0.01}	62.6 ^{+3.6} _{-3.0}	19.7 ^{+0.1} _{-0.1}	...	141.1/180
ZTF21abddofm	287.832023	-27.061537	9378.52 ^{+0.65} _{-0.68}	0.12 ^{+0.06} _{-0.06}	135.5 ^{+100.4} _{-37.5}	21.5 ^{+0.7} _{-0.5}	21.5 ^{+0.7} _{-0.5}	168.7/120
ZTF1917.5+4200	289.366518	42.002384	9009.74 ^{+0.28} _{-0.27}	0.42 ^{+0.03} _{-0.05}	24.0 ^{+2.1} _{-1.2}	19.5 ^{+0.2} _{-0.1}	19.9 ^{+0.2} _{-0.1}	2776.1/1220
ZTF20aculhzd	291.911991	26.802955	9205.41 ^{+0.74} _{-0.79}	0.06 ^{+0.06} _{-0.04}	58.2 ^{+6.7} _{-6.0}	19.9 ^{+0.2} _{-0.2}	20.9 ^{+0.2} _{-0.2}	1649.4/1283
ZTF18abnpead	294.720692	23.434248	8354.83 ^{+0.19} _{-0.18}	0.15 ^{+0.04} _{-0.04}	31.9 ^{+7.0} _{-4.6}	21.3 ^{+0.3} _{-0.3}	...	274.6/261
ZTF20abxwphk	298.009151	61.187181	9097.11 ^{+0.91} _{-1.04}	0.09 ^{+0.05} _{-0.03}	143.4 ^{+65.4} _{-41.9}	21.7 ^{+0.5} _{-0.5}	22.5 ^{+0.5} _{-0.5}	589.4/320
ZTF21aavany	298.067432	-1.789902	9267.84 ^{+5.07} _{-3.87}	0.15 ^{+0.12} _{-0.10}	142.2 ^{+42.4} _{-22.7}	21.2 ^{+0.5} _{-0.4}	21.8 ^{+0.5} _{-0.4}	332.7/251
ZTF18abmqxce	298.521686	13.042882	8274.98 ^{+0.14} _{-0.16}	0.10 ^{+0.03} _{-0.03}	28.7 ^{+7.6} _{-5.0}	21.0 ^{+0.4} _{-0.3}	21.0 ^{+0.4} _{-0.3}	1048.2/502
ZTF22aadgva	299.439097	29.956966	9610.62 ^{+2.75} _{-2.62}	0.58 ^{+0.27} _{-0.20}	175.0 ^{+41.8} _{-33.0}	19.3 ^{+0.6} _{-0.7}	21.3 ^{+0.6} _{-0.7}	1507.9/1271
ZTF21abrslijz	301.021801	21.649025	9444.77 ^{+0.19} _{-0.19}	0.19 ^{+0.02} _{-0.02}	16.1 ^{+1.8} _{-1.4}	20.3 ^{+0.2} _{-0.2}	...	900.4/586
ZTF20acvazdi	302.536856	36.942286	9223.33 ^{+0.44} _{-0.43}	0.02 ^{+0.02} _{-0.01}	96.7 ^{+5.9} _{-5.5}	19.8 ^{+0.1} _{-0.1}	21.6 ^{+0.1} _{-0.1}	5942.4/3504
ZTF19aaprjw	346.445080	40.109760	8574.39 ^{+1.87} _{-1.97}	0.15 ^{+0.03} _{-0.03}	87.6 ^{+11.3} _{-9.4}	20.5 ^{+0.3} _{-0.3}	21.5 ^{+0.2} _{-0.2}	1399.9/771

REFERENCES

- Bellm, E. C., Kulkarni, S. R., Graham, M. J., et al. 2019a, *PASP*, 131, 018002, doi: [10.1088/1538-3873/aaecbe](https://doi.org/10.1088/1538-3873/aaecbe)
- Bellm, E. C., Kulkarni, S. R., Barlow, T., et al. 2019b, *PASP*, 131, 068003, doi: [10.1088/1538-3873/ab0c2a](https://doi.org/10.1088/1538-3873/ab0c2a)
- Dekany, R., Smith, R. M., Riddle, R., et al. 2020, *PASP*, 132, 038001, doi: [10.1088/1538-3873/ab4ca2](https://doi.org/10.1088/1538-3873/ab4ca2)
- Duev, D. A., Mahabal, A., Masci, F. J., et al. 2019, *MNRAS*, 489, 3582, doi: [10.1093/mnras/stz2357](https://doi.org/10.1093/mnras/stz2357)
- Einstein, A. 1936, *Science*, 84, 506, doi: [10.1126/science.84.2188.506](https://doi.org/10.1126/science.84.2188.506)
- Foreman-Mackey, D., Conley, A., Meierjürgen Farr, W., et al. 2013, emcee: The MCMC Hammer, *Astrophysics Source Code Library*, record ascl:1303.002. <http://ascl.net/1303.002>
- Forster, F., Bauer, F. E., Pignata, G., et al. 2021, *Transient Name Server Discovery Report*, 2021-1034, 1
- Gould, A. 1994, *ApJL*, 421, L75, doi: [10.1086/187191](https://doi.org/10.1086/187191)
- . 2004, *ApJ*, 606, 319, doi: [10.1086/382782](https://doi.org/10.1086/382782)
- Graham, M. J., Kulkarni, S. R., Bellm, E. C., et al. 2019, *PASP*, 131, 078001, doi: [10.1088/1538-3873/ab006c](https://doi.org/10.1088/1538-3873/ab006c)
- Kim, D.-J., Kim, H.-W., Hwang, K.-H., et al. 2018, *The Astronomical Journal*, 155, 76, doi: [10.3847/1538-3881/aaa47b](https://doi.org/10.3847/1538-3881/aaa47b)
- Kim, S.-L., Lee, C.-U., Park, B.-G., et al. 2016, *Journal of Korean Astronomical Society*, 49, 37, doi: [10.5303/JKAS.2016.49.1.037](https://doi.org/10.5303/JKAS.2016.49.1.037)
- Kupfer, T., Prince, T. A., van Roestel, J., et al. 2021, *MNRAS*, 505, 1254, doi: [10.1093/mnras/stab1344](https://doi.org/10.1093/mnras/stab1344)
- Mao, S., & Paczynski, B. 1991, *ApJL*, 374, L37, doi: [10.1086/186066](https://doi.org/10.1086/186066)
- Masci, F. J., Laher, R. R., Rusholme, B., et al. 2019, *PASP*, 131, 018003, doi: [10.1088/1538-3873/aae8ac](https://doi.org/10.1088/1538-3873/aae8ac)
- Medford, M. S., Abrams, N. S., Lu, J. R., Nugent, P., & Lam, C. Y. 2023, *ApJ*, 947, 24, doi: [10.3847/1538-4357/acba8f](https://doi.org/10.3847/1538-4357/acba8f)
- Mróz, P., Udalski, A., Skowron, J., et al. 2017, *Nature*, 548, 183, doi: [10.1038/nature23276](https://doi.org/10.1038/nature23276)
- . 2019, *ApJS*, 244, 29, doi: [10.3847/1538-4365/ab426b](https://doi.org/10.3847/1538-4365/ab426b)
- Mróz, P., Udalski, A., Szymański, M. K., et al. 2020, *ApJS*, 249, 16, doi: [10.3847/1538-4365/ab9366](https://doi.org/10.3847/1538-4365/ab9366)
- Oke, J. B., & Gunn, J. E. 1982, *PASP*, 94, 586, doi: [10.1086/131027](https://doi.org/10.1086/131027)
- Paczynski, B. 1986, *ApJ*, 304, 1, doi: [10.1086/164140](https://doi.org/10.1086/164140)
- . 1996, *ARA&A*, 34, 419, doi: [10.1146/annurev.astro.34.1.419](https://doi.org/10.1146/annurev.astro.34.1.419)
- Poleski, R., & Yee, J. C. 2019, *Astronomy and Computing*, 26, 35, doi: [10.1016/j.ascom.2018.11.001](https://doi.org/10.1016/j.ascom.2018.11.001)
- Prochaska, J., Hennawi, J., Westfall, K., et al. 2020, *The Journal of Open Source Software*, 5, 2308, doi: [10.21105/joss.02308](https://doi.org/10.21105/joss.02308)
- Rodriguez, A. C., Mróz, P., Kulkarni, S. R., et al. 2022, *ApJ*, 927, 150, doi: [10.3847/1538-4357/ac51cc](https://doi.org/10.3847/1538-4357/ac51cc)
- Sajadian, S., & Poleski, R. 2019, *ApJ*, 871, 205, doi: [10.3847/1538-4357/aafa1d](https://doi.org/10.3847/1538-4357/aafa1d)
- Sumi, T., Udalski, A., Bennett, D. P., et al. 2016, *ApJ*, 825, 112, doi: [10.3847/0004-637X/825/2/112](https://doi.org/10.3847/0004-637X/825/2/112)
- Udalski, A., Szymański, M. K., & Szymański, G. 2015, *AcA*, 65, 1, doi: [10.48550/arXiv.1504.05966](https://doi.org/10.48550/arXiv.1504.05966)
- Udalski, A., Szymanski, M., Stanek, K. Z., et al. 1994, *AcA*, 44, 165, doi: [10.48550/arXiv.astro-ph/9407014](https://doi.org/10.48550/arXiv.astro-ph/9407014)
- Wyrzykowski, Ł., Rynkiewicz, A. E., Skowron, J., et al. 2015, *ApJS*, 216, 12, doi: [10.1088/0067-0049/216/1/12](https://doi.org/10.1088/0067-0049/216/1/12)
- Zang, W., Dong, S., Gould, A., et al. 2020, *ApJ*, 897, 180, doi: [10.3847/1538-4357/ab9749](https://doi.org/10.3847/1538-4357/ab9749)